INORGANIC CHEMISTRY
FRONTIERS

REVIEW

View Article Online
View Journal | View Issue

Cite this: *Inorg. Chem. Front.*, 2024, **11**, 3707

Prussian blue analogue-derived materials for photocatalysis

Xu Han,[a] Wen-Wen He,*[a] Tao Zhou[a] and Shengqian Ma *[b]

Prussian blue (PB) and Prussian blue analogues (PBAs), which are a family of coordination polymers (CPs), are considered excellent catalysts, and thus widely studied in the field of electrocatalysis. To date, numerous excellent studies on PBA-derived electrocatalysts have been reported. In contrast, in the field of photocatalysis, the exploration and reports on PBA and its derivatives are relatively scarce compared to electrocatalysis. However, in the past five years, an increasing number of PBA-derived photocatalysts has been reported in almost every field of photocatalysis. Due to their advantages of tailorable structures, favorable stability, low cost and simple preparation process, these materials show great potential in each field of photocatalysis. In this review, we summarize the latest developments in the synthesis and photocatalytic performance of PBA-derived photocatalysts. Our discussion is focused on PBA-derived photocatalysts in terms of photocatalytic hydrogen evolution, photocatalytic water oxidation, and CO_2 photoreduction. Subsequently, the design, catalytic performance and catalytic mechanism of PB/PBA-derived photocatalysts are discussed. Finally, the challenges and prospects in PB/PBA-derived materials for their application in photocatalysis and guiding principles for fabricating PBAs to realize distinguished activities are presented.

Received 7th March 2024,
Accepted 21st April 2024

DOI: 10.1039/d4qi00612g

rsc.li/frontiers-inorganic

1. Introduction

Nowadays, the increasing depletion of the traditional fossil energy sources and increased environmental problems have prompted researchers to devote more efforts to developing green and sustainable energy.[1,2] In this case, although wind energy, tidal energy and geothermal energy have been intro-

[a]*School of Chemistry and Life Science, Advanced Institute of Materials Science, Changchun University of Technology, Changchun 130012, China. E-mail: heww@ccut.edu.cn*
[b]*Department of Chemistry, University of North Texas, 1508 W. Mulberry St., Denton, TX 76201, USA. E-mail: Shengqian.Ma@unt.edu*

Xu Han

Xu Han received his MS Degree from Changchun University of Technology in 2023. He is currently a PhD candidate under the supervision of Wenwen He at Changchun University of Technology. His current research focuses on the preparation of Prussian blue analogues and covalent organic frameworks for application in photocatalytic hydrogen evolution.

Wen-Wen He

Wenwen He obtained her MS Degree from Northeast Normal University (NENU) in 2011 and graduated from NENU with a PhD Degree in 2016. In the same year, she joined the Changchun University of Technology as a Lecturer. In 2019, she joined Prof. Shengqian Ma's Group at the University of South Florida as a Visiting Scholar. She was promoted to Associate Professor in 2019. Her current research interest focuses on the development of POM-based materials, functional porous materials and Prussian blue analogues materials for application in catalysis, separation and energy storage.

duced in daily life gradually, the utilization of these energy sources usually requires large-scale harvesting devices.[3,4] The collected inexhaustible energy needs to be converted into electricity for transmission before use, and in fact there is usually a certain amount of transmission loss. In contrast, photocatalytic reactions allow solar energy to be directly collected and converted into usable substances in one step, endowing them broad application prospect in energy and material conversion.[5] As an effective measure for the utilization of solar energy, photocatalytic technologies have attracted significant interest, and many useful achievements have been made in photocatalytic hydrogen evolution, photocatalytic oxidation evolution, photocatalytic CO_2 reduction, nitrogen photo-fixation and so on.[6–8] However, significant hurdles such as poor solar efficiency, reaction selectivity and overall conversion rate affect the energy and material conversion promoted by solar-power energy. According to the literature, the solar conversion rate of different photocatalytic technologies has only reached 10%–20%, rarely exceeding 20%. Thus, to boost the energy utilization rate for photocatalytic reactions, the design and synthesis of high-efficiency photocatalysts have become particularly important. An efficient photocatalyst should overcome some deficiencies of existing materials, such as poor light harvesting capability, fast recombination of photo-generated electron–hole pairs (e–h), and lack of active sites.[9]

Accordingly, significant efforts have been devoted to promoting the catalytic activity and capacity of photocatalysts. The strategies reported thus far to build high-efficiency multifarious photocatalysts can be divided into three categories, as follows: (i) band structure regulation, (ii) morphology and size control of photocatalysts and (iii) surface modification.[10–12] These methods are different in terms of cost, operational difficulty and scope of application.

Shengqian Ma

Shengqian Ma obtained his B.S. Degree from Jilin University (China) in 2003, and graduated from Miami University (Ohio, USA) with a PhD Degree in 2008. After finishing a two-year Director's Postdoctoral Fellowship at Argonne National Laboratory, he joined the Department of Chemistry at University of South Florida as an Assistant Professor in 2010; he was promoted to Associate Professor with early tenure in 2015 and to Full Professor in 2018. In August 2020, he joined the University of North Texas as the Robert A. Welch Chair in Chemistry. His current research interest focuses on the task-specific design and functionalization of advanced porous materials for energy-, biological-, and environmental-related applications.

Semiconductors are good candidates for the design of photocatalysts, which possess conductivity between that of a conductor and insulator. Compared with metal conductors, semiconductors have a narrow band gap, endowing them with adequate photosensitive properties.[13] The TiO_2 semiconductor was first prepared to promote photocatalytic water splitting in 1972, and then the CdS semiconductor was first applied in photocatalytic reactions in 1977.[14,15] TiO_2 is a green catalyst with low cost and good stability. Alternatively, CdS has a strong visible light response, suitable band gap structure, and simple preparation process. However, their fast e–h recombination and light poisoning limit their wider application in photocatalytic reactions. Thus, new semiconductors have been created to accelerate the development of photocatalytic technologies, such as metal oxides, metal sulfides, g-C_3N_4, metal–organic frameworks (MOFs) and covalent organic frameworks (COFs).[16–25]

The following components play an important role in photocatalytic systems, including sacrificial reagents, REDOX media and photosensitive reagents.[26–28] (i) Sacrificial reagents. In n-type/p-type semiconductors, when light energy is absorbed, e^-/h^+ jump to the conduction band (CB)/valence band (VB) in the band gap of semiconductors. If these excited e^- and h^+ are not transferred immediately, they will return to the band gap and recombine with the rest of the species. In this case, the addition of sacrificial agents can combine the unused carriers in photocatalytic test systems to solve this problem and speed up the reaction. (ii) REDOX media. Photocatalytic reactions are often limited by their sluggish kinetics, and in this case, the addition of REDOX medium can accelerate the kinetics of the conversion process and promote faster charge transfer. (iii) Photosensitive reagents. Many semiconductors such as black materials have poor absorption and response capacity in the UV-visible region, and thus the addition of photosensitive reagents is the key to boosting their light absorption and light energy conversion efficiency.

To further increase the utilization rate of photo-generated electrons and prevent electron–hole recombination, the strategy of constructing heterogeneous structures has been applied in photocatalytic reactions.[27–29] The formation of heterostructures can not only achieve the effective separation of e^- and h^+, but also change the electronic property at the interface of different semiconductors to enhance their photocatalytic properties. There are three traditional heterojunctions, *i.e.*, straddling gap (type I) heterojunction, staggered gap (type II) heterojunction and broken gap (type III) heterojunction.[29] These traditional heterojunction types are all composed of two semiconductors with different valence and conduction band structures; meanwhile, the bandgaps of the two semiconductors overlap in different ways. In type III heterojunctions, they possess a non-overlapping band gap, which cannot transfer e^- and h^+ directly. Thus, only type I and type II heterojunctions can construct an effective heterostructure. In type I heterojunctions (Fig. 1a), the reduction reaction and oxidation reaction take place in the same semiconductor. In type II heterojunctions (Fig. 1b), the reduction reaction occurs on the

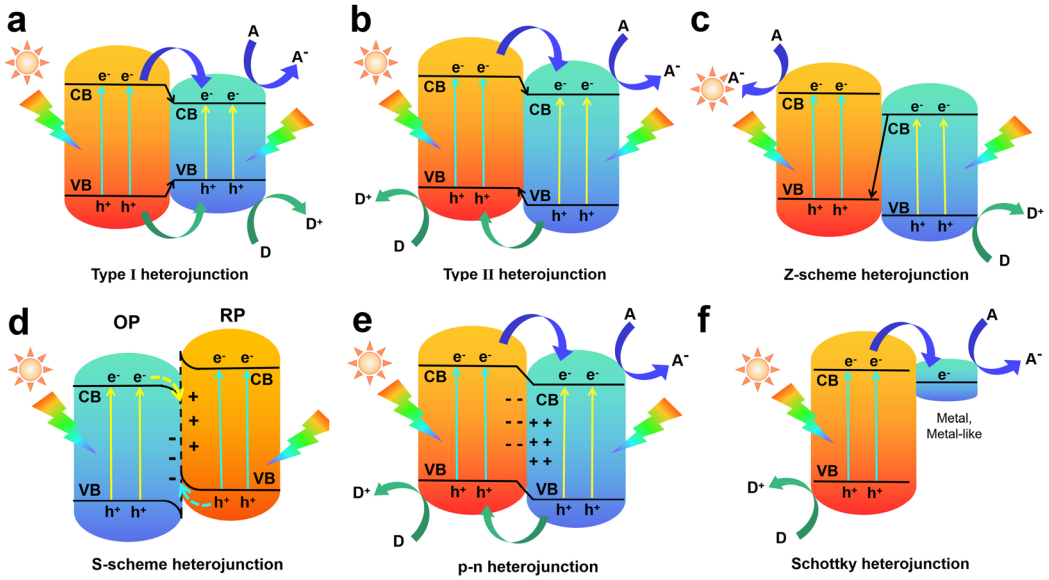

Fig. 1 Band structures of various types of heterojunctions. (a) Type I heterojunction, (b) type II heterojunction, (c) Z-scheme heterojunction, (d) S-scheme heterojunction, (e) p–n heterojunction, and (f) Schottky heterojunction.

semiconductor with a positive CB and VB, while the oxidation reaction occurs on the other semiconductor.

In recent years, several other types of heterojunctions have been reported (Fig. 1c–f), such as Z-scheme heterojunctions, S-scheme heterojunctions, p–n heterojunctions, and Schottky heterojunctions, respectively.[30–42] At present, Z-scheme and S-scheme heterojunctions have been studied in-depth and widely used for photocatalytic reactions. These heterojunctions are often constructed by distinct materials with different band gaps. (i) In 1979, Z-scheme heterojunctions were first reported by Bard, named after the "Z-type" electron transfer direction. In the original study, the formation of these heterostructure systems required the presence of REDOX. However, the light shielding effect, pH-sensitivity and poor stability of REDOX affected the application of Z-type heterojunctions. In 2013, a direct Z-scheme heterojunction complex was reported to overcome the shortcomings of the original Z-type heterojunction.[28,30–36] (ii) S-scheme heterojunctions are formed by reduced photocatalysts (RP) and oxidized photocatalysts (OP), which are similar to type II heterojunctions. However, the difference between type II and S-scheme heterojunctions is that a built-in electric field (BIEF) is formed in S-scheme heterojunctions, and the reduction and oxidation reactions occur on the RP and OP, respectively. At present, the S-scheme heterojunction photocatalysts are usually composed of two different n-type semiconductors with an obvious Fermi-level difference.[36–38] (iii) The p–n heterojunctions are constructed by n-type and p-type semiconductors, where the photo-excited e^- and h^+ will transfer from the n-type semiconductor to the p-type semiconductor to form a BIEF at the semiconductor interface. The p–n heterojunctions often appear in type I and type II heterojunctions.[39,40] (iv) Schottky heterojunctions are a special type of heterojunction made of a metal (Pt, Au, Ag, Ni, Co, *etc.*) or metal-like material (p-type metal sulfides, metal oxides, *etc.*) and a semiconductor or other heterojunctions, which are extensively used for electrocatalytic and photocatalytic reactions.[41,42] An in-depth analysis of the structural characteristics and internal electron flow of heterojunctions can help understand the electron transfer process in photocatalytic reactions, which is conducive to the design and synthesis of high-efficiency photocatalysts.

Prussian blue (PB) and Prussian blue analogues (PBA) are stable coordination polymers (CPs), which are similar but slightly different to MOFs. They are constructed by metal ions and transition-metal cyanometalates, having a three-dimensional (3D) angular cubic or two-dimensional (2D) lamellar structure.[43–47] The discovery of PB can be traced back to the early 18th century, which was the first coordination compound to be discovered. Originally, PB was used as a dye in Berlin, Kingdom of Prussia.[48] The coordination metals of PB at that time were Fe ions. Unless otherwise indicated, PB and PBAs are collectively referred to as PBAs in this review. The general formula of PBAs is $A_xM_a[M_b(CN)_6]_y{\cdot}zH_2O$, where the A_x are cations intercalated between the frameworks and M_a and M_b the metal ions coordinated to the cyano groups.[49] Besides an adjustable nanoscale structure, PBAs have merits such as favorable stability, low cost and simple preparation. Due to these advantages, PBAs have been applied in various fields such as batteries, cells, electrodes, catalysis, and nanoenzymes (Fig. 2). According to our search on "*Web of Science*" using the keyword PBAs, more than 7900 articles were reported up to the end of December 2023. To date, there are over 30 reviews in the field of electrocatalytic water splitting related to PBAs. However, there is no review focusing on the application of PBAs in photocatalysis.

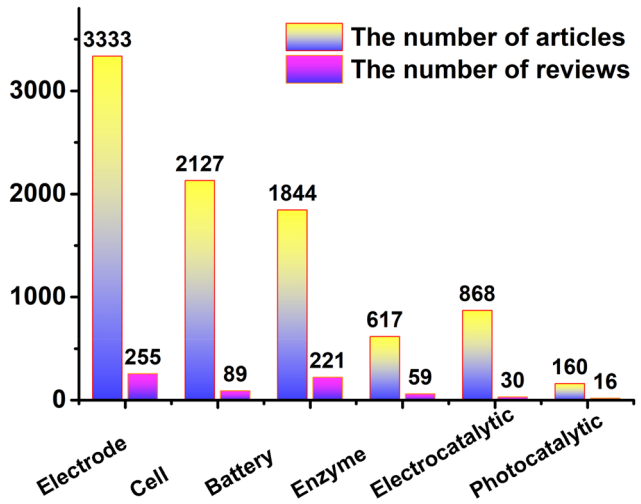

Fig. 2 Number of articles on Prussian blue in different fields up to the end of December 2023, data from the "*Web of Science*".

PBAs and their derived materials have been widely applied in various photocatalytic reactions.[50–53] In this review, we summarize the recent progress on PBA-derived materials in three main types of photocatalytic reactions, which are photocatalytic H_2 evolution, photocatalytic O_2 evolution and CO_2 photoreduction reactions respectively (Fig. 3). Firstly, we discuss the widely used systems for photocatalytic reactions and summarize the suitable test systems for PBA-derived photocatalysts. Then, we focus on a systematic discussion on PBA-derived materials regarding their synthesis strategy, metal regulation, morphology regulation, heterogeneous structure construction, enhanced photocatalytic performance and correlation between their structure and activity. Finally, some existing scientific challenges, future development directions and perspective towards opportunities for PBA-derived photocatalysts will be described.

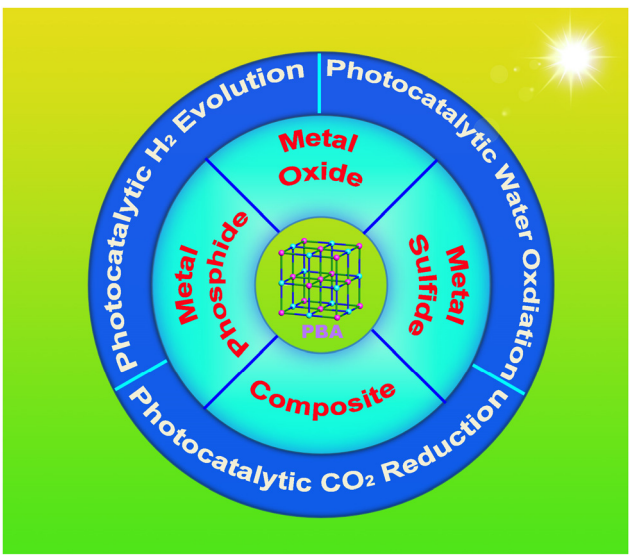

Fig. 3 Various types of PBA-derived catalysts for photocatalytic reactions.

2. Test system for photocatalytic reactions

The methods for converting light energy into chemical energy are first derived from the process of photosynthesis. In green plants, several organelles and enzymes are involved in the process of photosynthesis. Thus, researchers usually add some necessary auxiliary components to photocatalysis systems to mimic the role of the above-mentioned organelles.[54–56] In the test systems of PBAs and their derived photocatalysts, it is necessary to choose suitable REDOX media, sacrificial agents and photosensitizers to enhance their photocatalytic performance.

2.1. REDOX medium for photocatalytic reaction

In the first stage of photosynthesis, light-dependent reactions of photosynthesis systems have two important components, *i.e.*, PSI (product hydrogen protons) system and PSII (applied for oxygen evolution) system, as shown in Fig. 4.[57] The invention of PEC cells is inseparable from the inspiration of photosynthesis. Mimicking these systems, hybrid photoelectrochemical (PEC) cells have been designed with REDOX media to drive photocatalytic water splitting.[58] REDOX media as an auxiliary for electron transfer have been widely applied in different photocatalytic reactions. IO^{3-}/I^- (I^{3-}/I^-), Ru^{3+}/Ru^{2+}, $[Co(bpy)_3]^{3+/2+}$ and Fe^{3+}/Fe^{2+} are the commonly used REDOX

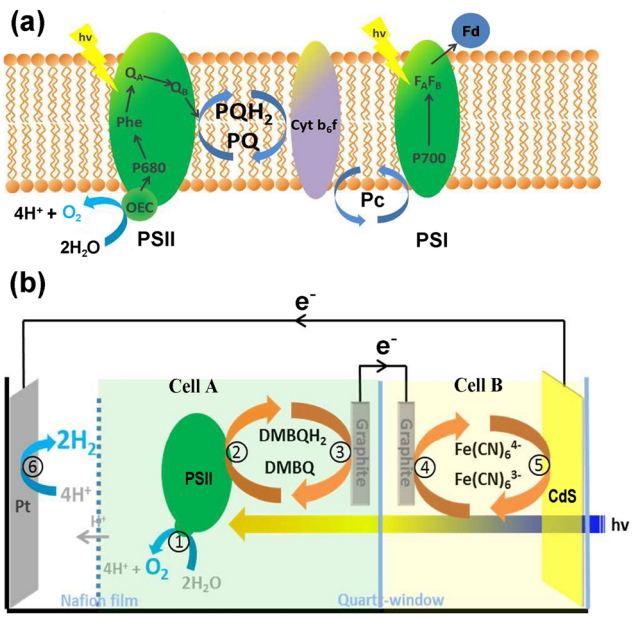

Fig. 4 (a) Schematics of the electron transfer path from PSII to PSI in natural photosynthesis. (b) Schematics of the CdS–PSII hybrid PEC battery and the brief instruction of the electron transfer path. Reproduced with permission from ref. 57. Copyright 2019, The Royal Society of Chemistry.

media at present.[59–65] These REDOX media are often formed by adding their chemical solution to the photocatalytic reaction systems directly. Besides, REDOX media can also assist to construct liquid-phase Z-scheme photocatalytic systems. The robust structure of PBAs are formed by a cyano group and metal ions of different valence states (M_a^{2+}–C≡N–M_b^{3+}), which can make them become favorable REDOX media for photocatalytic reactions to build Z-scheme systems. However, although REDOX media can improve the reaction conversion efficiency, most of them will hinder the light absorption of semiconductors and easily lose their activity in strong acid or base conditions. Meanwhile, these REDOX media can only be used in the liquid phase.[61] In 2021, Mei and Hang *et al*. found that a Cu–Fe PBA could be used as solid-state REDOX mediator to drive the water electrolysis process, indicating that PBAs have a good potential for the construction of all-solid-state Z-scheme photocatalytic systems.[64]

2.2. Sacrificial agents for photocatalytic reactions

In photocatalytic reactions, the photo-electrons and holes created by semiconductors will immediately recombine if they are not transferred immediately. Thus, to make greater use of photo-generated electrons or holes efficiently, it is necessary to add suitable sacrificial agents to accept the residual photo-holes or electrons. There are two type of sacrificial agents, electron donors and electron receptors, respectively.[66] The sacrificial electron donors are usually used in reduction reactions (H_2 evolution and CO_2 reduction), and sacrificial electron acceptors are usually used in oxidation reactions (O_2 evolution).

In the case of n-type semiconductors, electron donors can occupy the h^+ generated by photo-excitation, preventing the e^- from returning to the conduction band and recombining with the h^+. Regarding p-type semiconductors, electron receptors are often combined with e^- to promote photocatalytic reactions. At present, methanol, triethanolamine (TEOA), ethylene diamine tetraacetic acid (EDTA), L-lactic acid (LA), L-ascorbic acid (AA) or its sodium salt, and sodium sulphide/sodium sulfite complex salt are popular sacrificial agents.[66–72] Bahruji *et al*. studied 20 different sacrificial agents and proved that these sacrificial agents can all increase the efficiency of photocatalytic hydrogen evolution.[71] The catalytic activities of different alcohols follow the order of triol > diol > primary alcohol > secondary alcohol > tertiary alcohol. Because PBAs can remain stable under highly acidic conditions, most acid sacrificial agents can be applied in photocatalytic systems with PBAs and PBA-derived photocatalysts.[73] In some alkaline-stable PBA-derived materials, such as metal sulfides, nitrides, and phosphates, or other PBA-containing composite materials, TEOA and TEA can be used. In addition, Na_2S/Na_2SO_3 and $Na_2S_2O_8$ are also frequently used as sacrificial agents for PBA-derived photocatalysts.

2.3. Photosensitizers for photocatalytic reactions

Compared to sacrificial agents and REDOX media, photosensitizers are the most important components for photocatalytic reactions. Most PBAs and their derived photocatalysts have weak light absorption capacity in the visible-light region, causing them to poorly utilize light energy.[74] Some photosensitive substances can help overcome this problem. They can be absorbed on the surface of photocatalysts to increase their light absorption capacity, which are named photosensitizers. At present, the commonly used photosensitizers are eosin Y (EY) and its analogues, tris(2,2′-bipyridyl) ruthenium(III) (RuBpy) and its analogues, porphyrins and phthalocyanines.[74–80] Most of them are directly added to photocatalytic systems, while some of them are grafted onto semiconductor materials. In some cases, photocatalysts are composed of photosensitizers. At present, the most common photosensitizers used for PBAs and their derived photocatalysts are EY and RuBpy.

In the photocatalytic systems with TEOA, EY is a commonly used photosensitizer, which can be turned into an excited state after absorbing light energy, and then converted into a trilinear state ($EY^{3}*$). Meanwhile, TEOA is oxidized to $TEOA^+$, thereby assisting $EY^{3}*$ to convert into EY^-. Finally, the photo-electrons are transferred to the photocatalyst and the EY^- will return to the ground state (EY).[77] However, with the consumption of TEOA, the reaction rate will decrease in this system. The further addition of sacrificial agents can maintain the reaction rate. Besides, RuBpy and $Na_2S_2O_8$ are often used together in photocatalytic reaction systems. In this system, $[Ru(bpy)_3]^{2+}$ first absorbs photons and changes into the excited state of $[Ru(bpy)_3]^{2+}*$. Photogenerated oxidant $[Ru(bpy)_3]^{3+}$ is formed through the transfer of electrons from $[Ru(bpy)_3]^{2+}*$ to $S_2O_8^{2-}$. After that, $[Ru(bpy)_3]^{3+}$ oxidizes the catalyst to high-valence species and $Na_2S_2O_8$ will be reduced to Na_2SO_4. Then, $Ru(Bpy)_3^{3+}$ will return to $Ru(Bpy)_3^{2+}$. In this process, a hole will be generated, which can move to the surface of photocatalysts to drive oxidation reactions.[78–80] However, the high cost of RuBpy hinders its wide use in photocatalytic systems, and it is only widely used in the water oxidation process.

Thus, to improve light response of PBA materials, the strategy of adding photosensitizers to the test systems directly is commonly used in numerous cases. However, the use of this approach usually makes it difficult to recycle the photosensitizer, which may cause environmental pollution simultaneously. Accordingly, connecting photosensitive groups to the PBA framework can solve this problem, building a polymeric platform for PBAs and photosensitizers to effectively improve the light absorption capacity of the compound.

3. PBA-derived materials for photocatalysis

PBAs and their derived materials have multiple and various electronic and band gap structures, which will usually affect the charge transfer direction and charge transfer ability of a composite photocatalyst in photocatalytic H_2 evolution, photocatalytic water oxidation and CO_2 photoreduction reactions. In the photocatalytic H_2 evolution and CO_2 photoreduction reac-

tions, the charge transfer mechanisms have four steps, as follows: (i) absorbing light energy to create excitons. (ii) The dissociation of excitons into e^- and h^+. (iii) A carrier made up of e^- migrates to the surface active sites of the semiconductor to participate in the reduction reaction, and the h^+ remaining on VB can subsequently combine with electron donors. (iv) The evolution of the reduction products on the surface of the catalyst. Similarly, the charge transfer mechanism for photocatalytic water oxidation reactions also involves the above-mentioned four steps. In photocatalytic water oxidation reactions, the difference is that e^- will combine with electron receptors and the h^+ will move to surface active sites to evolve oxidation from water.[5–10] In these photocatalytic reactions, it is important to select photocatalysts with suitable band gaps.[81] As shown in Fig. 5a, the E_{CB} for H_2 evolution photocatalysts should be more negative than −0.41 V *vs.* NHE at pH = 7 and the E_{VB} for water oxidation photocatalysts should be more positive than +0.82 V *vs.* NHE at pH = 7. Due to the fact that the E_{CB} for different products is quite close, the accurate design of the E_{CB} of photocatalysts is a good way to improve the selectivity for CO_2 photoreduction reactions. The above-mentioned band gap potentials can be determined by Mott–Schottky, VB-XPS, UPS and UV-vis DRS and other characterizations, helping calculate the band gap of PBA-derived photocatalysts (Fig. 5b). Besides, single PBAs have a poor photo-response and photo-stability, which hinder their application in these photocatalytic reactions. Thus, many strategies have been designed to overcome the above-mentioned obstacles, as follows: (i) adding a photosensitizer to the photocatalytic reaction system. (ii) Constructing metal sulfide or metal phosphide photocatalysts by using PBAs as precursors to control the morphology and band gap of PBA-derived photocatalysts. (iii) Constructing composite materials to form heterogeneous structures.

3.1. PBAs and their derived materials as photocatalysts for photocatalytic hydrogen evolution

In photocatalytic hydrogen evolution (PHE) reactions, PBA-derived photocatalysts usually have suitable band gap structures and excellent photo-stability. As remarkable precursors or substrates, PBAs can become efficient hydrogen evolution photocatalysts through metal or morphology regulation (a summary of different PBA-based photocatalysts for hydrogen evolution is presented in Table 1). The application of PBA-derived photocatalysts can be divided into three main types, as follows: (i) as REDOX media to drive photocatalytic hydrogen evolution; (ii) excellent precursor for metal sulfides or phosphides, where PBA-derived metal sulfides and phosphides are high-efficiency catalysts for photocatalytic hydrogen evolution; and (iii) PBAs and their derived materials used to construct composite photocatalysts for photocatalytic hydrogen evolution.

3.1.1. PBA-based REDOX media. As a primary component of PB, hexacyanoferrates with different valences were first used as REDOX media for photocatalytic H_2 evolution reactions in 2014.[82,105] After a long time, this type of REDOX medium was used in the PSII system with traditional photo-electrodes composed of Pt/CdS materials in 2017.[57] However, the exploration of catalytic mechanisms between Pt/CdS and hexacyanoferrate are not thorough. In the same year, Abe and Higashi proposed an all-purpose strategy to reveal the catalytic mechanism between metal sulfides (CdS, $ZnIn_2S_4$ and $CdIn_2S_4$) and the $[Fe(CN)_6]^{3-/4-}$ REDOX medium in Z-scheme water splitting systems (Fig. 6).[83] They demonstrated for the first time that $[Fe(CN)_6]^{3-}$ will be generated from $[Fe(CN)_6]^{4-}$ during the progress of H_2 evolution. This backward reaction may gradually decrease the rate of H_2 evolution. Besides, there is a photo-absorption peak at around 420 nm for $[Fe(CN)_6]^{4-}$, and the light shielding effect of $[Fe(CN)_6]^{4-}$ can also inhibit the H_2 evolution. Compared with $ZnIn_2S_4$ and $CdIn_2S_4$, Pt/CdS have a fast photo-corrosion progress, which may spontaneously form $K_2[CdFe(CN)_6]$ layers on Pt/CdS, resulting in a higher H_2 evolution rate of 67.7 μmol h^{-1} (1.354 μmol g^{-1} h^{-1}). Subsequently in 2018, to further explore the influence of REDOX media on Pt/CdS, Kato and Kobayashi used a series of hexacyanidometallate ($[M(CN)_6]^{4-}$, M = Fe or Ru) PBA REDOX to modify the Pt/CdS nanorod photocatalyst.[84] Because the Ru(III)/Ru(II) potential of CdRu–PW (+1.42 V *vs.* NHE) is closer to the VB potential of CdS–NR (+1.7 V *vs.* NHE), $[Ru(CN)_6]^{4-}$ is a more suitable REDOX medium for Pt/CdS photocatalysts, which can act as an electron source for the photocatalytic H_2 evolution reaction (Fig. 7).[85] In the presence of $[Ru(CN)_6]^{4-}$, Pt/CdS–NR catalysts can produce about 1.2 μmol H_2 in 6 h (100 μmol g^{-1} h^{-1}).

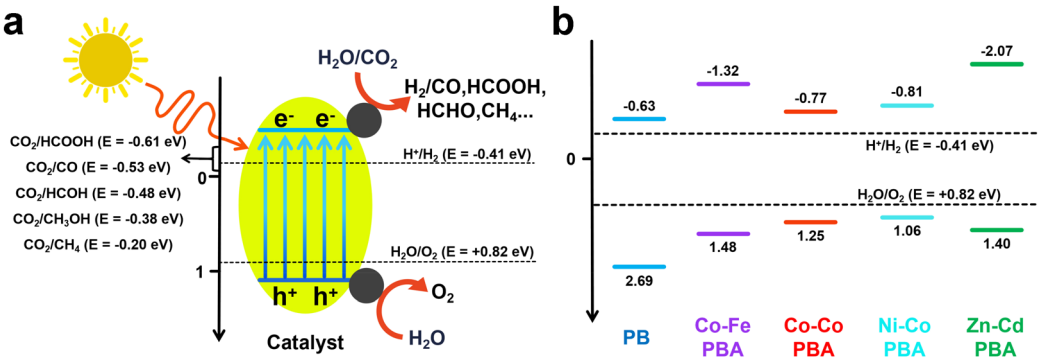

Fig. 5 (a) REDOX potentials of different species for photocatalytic reactions. (b) Band gap structures of different PBAs.

Table 1 Summary of different PBA-based photocatalysts for hydrogen evolution

Material	Irradiation	Sacrificial agent	REDOX medium	H_2 evolution rate/(mmol g^{-1} h^{-1})	Ref.
Pt/CdS	$\lambda > 420$ nm	None	$[Fe(CN)_6]^{3-/4-}$	8.85	82
Pt/CdS	$\lambda \geq 400$ nm	None	$[Fe(CN)_6]^{3-/4-}$	1.35	83
Pt/CdS–NR	$\lambda = 470 \pm 10$ nm	None	$[Ru(CN)_6]^{3-/4-}$	1.73	84
InHCF/RCO/TaON	$\lambda > 400$ nm	None	Fe^{3+}/Fe^{2+}	2.08	85
yolk–shell CdS	$\lambda \geq 420$ nm	Na_2S/Na_2SO_3	None	3.05	86
CdS frame-in-cage	$\lambda \geq 400$ nm	Na_2S/Na_2SO_3	None	13.6	87
$Cd_{0.5}Zn_{0.5}S$	$\lambda \geq 420$ nm	Na_2S/Na_2SO_3	None	4.34	88
ZnCdS	$\lambda \geq 420$ nm	Na_2S/Na_2SO_3	None	23	89
ZnCdS	$\lambda \geq 420$ nm	Na_2S/Na_2SO_3	None	21	90
Ni_xCd_yS	$\lambda \geq 420$ nm	Na_2S/Na_2SO_3	None	8.45	91
Co–FeP@NC-4	$\lambda \geq 420$ nm	TEOA	None	13.3	92
NCP-60	$\lambda \geq 420$ nm	TEOA	None	16.6	93
$TiO_2/Cu_3[Co(CN)_6]_2$	$\lambda > 420$ nm	TEOA	None	2.86	94
PBA–TiO_2	$\lambda > 420$ nm	$TEOA/NaIO_3$	None	0.198	95
g-C_3N_4–Fe_2N	$\lambda \geq 420$ nm	TEOA	None	0.0887	96
$NiCo_2O_4$@GDY	$\lambda \geq 420$ nm	TEOA	None	4.84	97
PB–Co/CdS–LT-3	$\lambda \geq 420$ nm	LA	None	57.22	98
CdS/ZnCd–PBA	$\lambda \geq 420$ nm	LA	None	19.24	99
ZnCdS/NiCoP	$\lambda \geq 420$ nm	LA	None	11.66	100
H–NCP/H–ZCS	$\lambda > 420$ nm	Na_2S/Na_2SO_3	None	73	101
$ZnIn_2S_4$/CdS	$\lambda \geq 420$ nm	Na_2S/Na_2SO_3	None	7.4	102
CN-2	$\lambda \geq 420$ nm	Na_2S/Na_2SO_3	None	44.4	103
Ni_3FeN	$\lambda > 400$ nm	TEOA	None	16.96	104

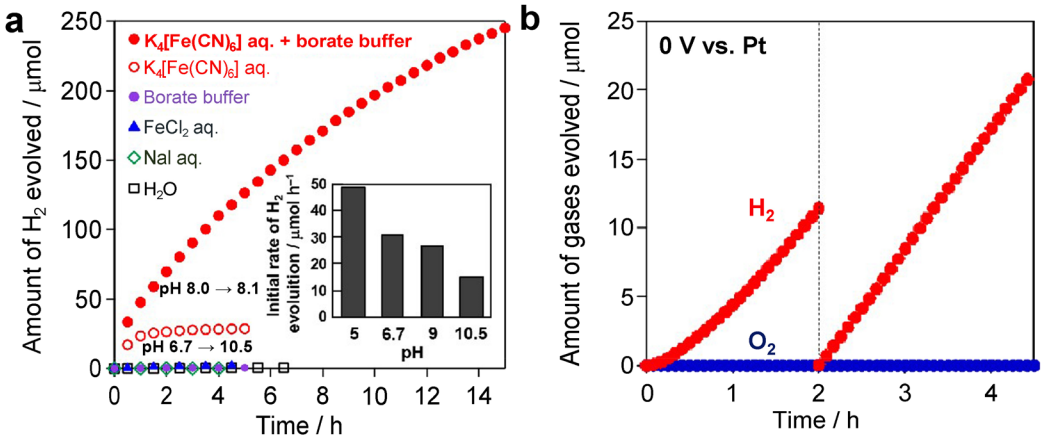

Fig. 6 (a) H_2 evolution yields for Pt/K_2[CdFe(CN)$_6$]/$ZnIn_2S_4$ under different reaction conditions. (b) Time courses of Z-scheme water splitting system using Pt/K_2[CdFe(CN)$_6$]/$ZnIn_2S_4$ as H_2-evolving photocatalysts. Reproduced with permission from ref. 83. Copyright 2017, The Royal Society of Chemistry.

Inspired by the above-mentioned strategies, in 2023, a strategy of surface modification of a RCO/TaON ($Rh_xCr_{2-x}O_3$ denoted as RCO) electrode with metal hexacyanoferrates (MHCF, M = Cd^{II}, Zn^{II}, or In^{II}) was reported. MHCF can combine with the added Fe^{3+}/Fe^{2+} to form a REDOX medium, helping to release RCO from the electrode to combine H^+ and generate H_2. Compared with the unmodified RCO/TaON electrode, the InHCF/RCO/TaON electrode can drive a significantly higher H_2 evolution rate (104 μmol h^{-1}).[86] This work proved that InHCF nanoparticles can be regarded as solid electron mediators for achieving a Z-scheme system.

3.1.2. PBA-derived metal sulfides and phosphides for photocatalytic H_2 evolution. Metal sulfides are the best candidate materials for photocatalysts because of their narrow band gap and remarkable photoresponse. Before the appearance of MOFs and COFs, CdS was extensively studied because of its obvious advantages such as good light absorption ability, high stability and appropriate band gap (2.4 eV) structures.[86] The earliest application of CdS in photocatalytic water splitting was in 1981.[87] Here, a platinized cadmium sulfide composite (Pt/CdS) was synthesized and first applied as a catalyst for photocatalytic H_2 production, achieving the H_2 evolution rate of 694 μmol g^{-1} h^{-1}.[88] Since then, CdS-based catalysts have been widely used for photocatalytic H_2 production.[89]

PBA can provide abundant metal sources for PBA-derived sulfides. Further, as excellent robust framework materials, the morphology of PBA-derived sulfides can be well regulated through the material synthetic progress. Accordingly, many

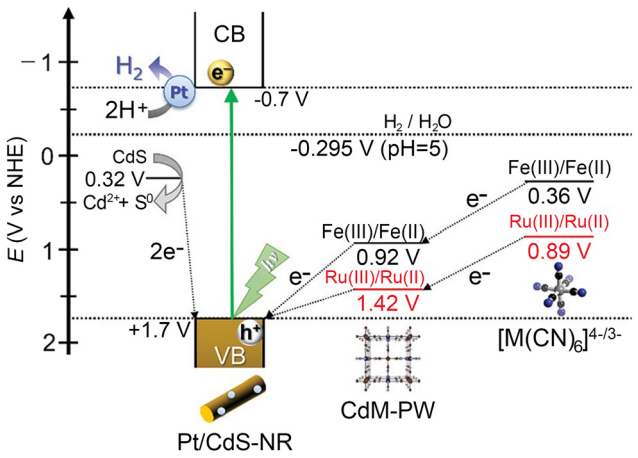

Fig. 7 Schematic energy diagram for the photocatalytic H_2 evolution reaction driven by Pt/CdS–NR in the presence of $K_4[M(CN)_6]$ (M = Fe or Ru) REDOX mediators. Reproduced with permission from ref. 84. Copyright 2018, The Royal Society of Chemistry.

fantastic structures have been obtained, such as hollow case structures, hollow frame structures, and frame-in-cage structure.[43–45] These structures can not only greatly increase the specific surface area of materials, but also help expose more active sites for subsequent reactions. The first application of a PBA-derived CdS material for photocatalytic hydrogen evolution was only recently reported in 2017.[90] In this report, Wang and Liu designed a yolk–shell CdS microcube with Cd–Fe PBA and Na_2S. The etching equation is $Cd_3[Fe(CN)_6]_2 + S^{2-} \rightarrow 3CdS + 2[Fe(CN)_6]^{3-}$. Due to the different diffusion abilities of Cd^{2+} and S^{2-}, the CdS shell and the Cd–Fe PBA core were initially formed. As the etching proceeds, S^{2-} spreads inward and combines with the inner Cd^{2+} to form a CdS nucleus. Then, hollow yolk–shell CdS microcubes are obtained. This hollow yolk–shell CdS microcube achieved an H_2-production rate of 3.05 mmol $h^{-1}g^{-1}$, which is 2.43 times higher than that of the pure CdS particles. Likewise, Lou prepared individual CdS frame-in-cage particles in 2020 inspired by PBA-based electrocatalysts.[91,92] The CdS frame-in-cage particles were constructed through a facile two-step sulfidation. Similar to the synthetic strategy of yolk–shell CdS microcubes, CdS frame-in-cage particles were also obtained by etching Cd-doping PBA (Cd–Co PBA). However, the sulfuration process of CdS frame-in-cage particles is different from yolk–shell CdS microcubes. In the first step, thioacetamide (TAA) and ammonia water are used as etching reagents. Then, Na_2S is applied as an etching reagent in the second sulfuration. This mild reaction process allows PBA to exist in the frame-in-cage structure. The thin shells outside the CdS frame-in-cage particles can accelerate the separation of photoelectrons and holes, achieving a high hydrogen production rate of 13.6 mmol g^{-1} h^{-1}. The hollow structures in the above-mentioned two photocatalysts not only endowed these materials with a large specific surface area and abundant active sites, but also enhanced light-absorption capability due to the light scattering effect.

Numerous bimetallic sulfide photocatalysts have been prepared by etching PBAs with different metals. In 2020, Liu designed a type of mono-disperse $Cd_{0.5}Zn_{0.5}S$ nanospheres ($Cd_{0.5}Zn_{0.5}S$–S) *via* the solvothermal route.[93] $Cd_{0.5}Zn_{0.5}S$–S was obtained by etching a Cd–Zn–Fe PBA material with TAA.[93] The photocatalytic H_2 evolution rates of $Cd_{0.5}Zn_{0.5}S$–S and $Cd_{0.5}Zn_{0.5}S$ nanoparticles ($Cd_{0.5}Zn_{0.5}S$–P, synthesized by direct method) were 4.34 and 2.07 mmol g^{-1} h^{-1}, respectively. Compared with $Cd_{0.5}Zn_{0.5}S$–P, $Cd_{0.5}Zn_{0.5}S$–S has many advantages, such as nano-spherical morphology, larger specific surface area and stronger light absorption capacity. This work provides an idea for the preparation of PBA-derived bimetallic sulfide photocatalysts. In 2022, Tsubaki and Jin obtained a hollow ZnCdS particle cage by modifying a Zn–Cd–Co PBA with ammonia and TAA as etching and sulfurizing reagents, respectively.[94] In this study, there are three type synthesis routes for ZnCdS with various shapes, including ZnCdS bulk, ZnCdS cage and hollow ZnCdS cage (Fig. 8). The hollow ZnCdS

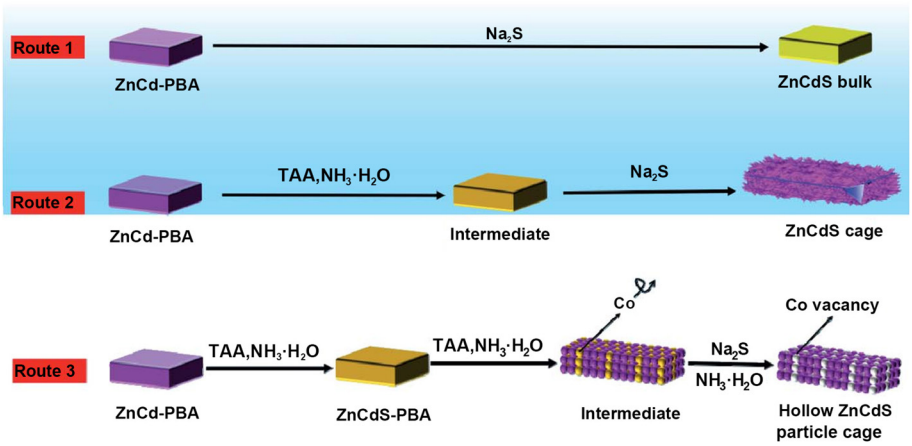

Fig. 8 Schematic illustration of the synthesis of Zn–Cd PBA-induced ZnCdS derivatives *via* different routes. Reproduced with permission from ref. 94. Copyright 2022, The Royal Society of Chemistry.

cages could achieve a comparatively higher photocatalytic H_2 evolution rate of 23.18 mmol g^{-1} h^{-1} under a 300 W Xenon lamp. After 4 cyclic photocatalytic hydrogen evolution tests, only a slight decrease in the H_2 evolution rate was observed, indicating the excellent good stability of the hollow ZnCdS cages. In the same year, this group reported a similar study on bimetallic sulfides, as shown in Fig. 9.[95] They prepared a series of metal sulfides using PBAs as the precursor, including CdS, MnCdS, and ZnCdS, to explore the effect of different metal dopants on the morphology and band gap structure of the sulfides. Among them, only ZnCdS possess a hollow structure and achieved an H_2 production rate of 21 mmol g^{-1} h^{-1}. The results indicated that ZnCdS and MnCdS both have a narrow band-gap and a negative flat band potential (E_{FB}) compared with CdS. In contrast, the E_{FB} of ZnCdS is more negative, which can result in a higher driving power to support a better photocatalytic performance. In summary, constructing hollow structures is a good method to improve the photocatalytic reaction activity of PBA-derived materials and the application of mild etching methods can better transform PBAs into well-structured hollow metal sulfides.

In 2021, Wang and Guo prepared a series of Ni_xCd_yS photocatalyst by nickel doping using Ni–Cd–Co PBA and Na_2S.[96] The chemical equation is $Ni_xCd_y[Co(CN)_6]_2 + S^{2-} \rightarrow Ni_xCd_yS + [Co(CN)_6]^{3-}$. The Ni_1Cd_2S photocatalyst could achieve the H_2 yield of 8.45 mmol g^{-1} h^{-1}, which was three times higher than that of pure CdS. The test results showed that this tiny doping content of Ni can effectively enhance the fluorescence lifetime of the Ni_1Cd_2S photocarriers, reducing the recombination rate of the photo-generated electrons and holes.

Metal phosphides are a good type of noble metal-free catalysts for photocatalytic H_2 evolution.[97] In comparison to traditional metal phosphides, PBA-derived metal phosphides have some unique properties, such as enhanced light absorption capacity, fast photo-generated charge transfer ability, low overpotential for HER and high stability in photoreactions. Further, PBA-derived metal phosphides usually have hollow structures, which are beneficial for photocatalytic H_2 evolution.

In 2022, Jin and Hao designed and synthesized a variety of ultrathin nitrogen-doped carbon Co–FeP (Co–FeP@NC).[98] By regulating the growth kinetics, Co–Fe PBA precursors with three types of shapes were obtained, including cage, frame and box shapes. After phosphating, these shapes were preserved in Co–FeP@NC materials. All these Co–FeP@NC materials have a remarkably enhanced light absorption capacity compared to Co–Fe PBA precursors. Among them, the Co–FeP@NC cages have a narrowest band gap and highest separation efficiency of electron–hole pairs, achieving the H_2 evolution rate of 13.31 mmol h^{-1} g^{-1} in TEOA aqueous solution.

Employing different modification strategies, Tsubaki and Jin obtained a series photocatalysts including CoO_3/NiO compounds, NiCoP nanoparticles, and $CoNi_2S_4$ nanorods in 2023.[99] In this work, the Ni–Co PBA was first etched by NH_4OH

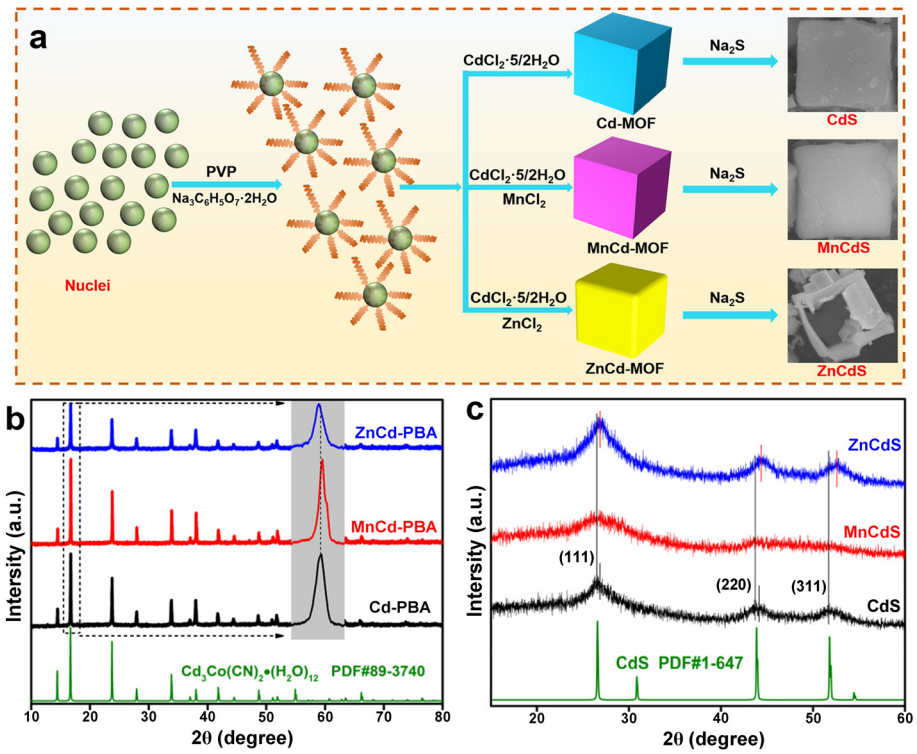

Fig. 9 (a) Schematic illustration of the growth mechanism for the formation of Cd–PBA, MnCd–PBA, ZnCd–PBA and their sulfide derivatives. (b) XRD patterns of Cd–PBA, MnCd–PBA, and ZnCd–PBA. (c) PXRD patterns for CdS, MnCdS, and ZnCdS. Reproduced with permission from ref. 95. Copyright 2022, The Royal Society of Chemistry.

at different etching times to obtain a precursor named NCP-x (x = 0, 30 and 60). After that, NCP-60 was used for the preparation of CoO_3/NiO compounds, NiCoP nanoparticles, and $CoNi_2S_4$ nanorods. CoO_3/NiO compounds were obtained by annealing treatment of NiCoP nanoparticles and $CoNi_2S_4$ nanorods were obtained by solvothermal reaction. The performance of these catalysts was higher than that of Ni–Co PBA, and the NiCoP nanoparticles achieve the fastest H_2 evolution rate of 15 mmol h^{-1} g^{-1} in TEOA aqueous solution. This work indicated that the photocatalytic activity of PBA-derived metal phosphides with a hollow structure is better than that of solid structures.

In summary, sulfuration and phosphating are two effective strategies for the preparation of PBA-derived photocatalysts. However, the research on PBA-derived materials applied as photocatalysts is still scarce thus far. There diverse technologies and reagents for sulfurizing and phosphating materials. In this case, a reasonable preparation method that mimics PBA-derived electrocatalysis will greatly promote the preparation of PBA-derived photocatalysts.

3.1.3. PBA-derived composites for photocatalytic H_2 evolution. To improve the photocatalytic performance of PBA materials, PBA-derived composites have been designed and synthesized. Various synthetic methods, such as self-assembly, hydrothermal/solvothermal, and chemical precipitation methods, have been reported.[100] TiO_2 and carbon nitride (g-C_3N_4) are the most popular substrate materials for photocatalysts because of their excellent 2D structure and good chemical stability. In 2020, Reguera and Pena reported the synthesis of a TiO_2/$Cu_3[Co(CN)_6]_2$ composite obtained from $Cu_3[Co(CN)_6]_2$ and TiO_2 *via* an ordinary chemical precipitation method.[101] The TiO_2/$Cu_3[Co(CN)_6]_2$ composite exhibited a high hydrogen evolution rate of 2.86 mmol h^{-1} g^{-1}, surpassing that of pure TiO_2 by 16 times. The TiO_2/$Cu_3[Co(CN)_6]_2$ composite possessed a high specific surface area and suitable band gap. However, $Cu_3[Co(CN)_6]_2$ in the composite may easily turn into $Co(OH)_2$ and $Cu(OH)_2$, causing a slight decrease in its photocatalytic performance after several reuses. In 2021, a PBA–TiO_2 Janus nanoreactor was prepared using Ni–Co PBA and 2D TiO_2,[102] which involved three key steps. Firstly, the Ni–Co PBA precursor with unsaturated metal sites was obtained by mild etching. Then, some TiO_x was embedded on the surface of the Ni–Co PBA precursor. Finally, TiO_x evolved into free-standing flowers on the surface of Ni–Co PBA using ethylene glycol and CH_3COOH as morphology control agents. This PBA–TiO_2 Janus nanoreactor achieved a higher photocatalytic H_2 evolution (198 μmol g^{-1} h^{-1}) and O_2 evolution (168 μmol g^{-1} h^{-1}) performance with different sacrificial agents compared with Ni–Co PBA and TiO_2 alone. The special interfacial structure in the PBA–TiO_2 Janus nanoreactor is a type II heterojunction. The construction of heterojunction plays a crucial role in the subsequent separation and transfer of photo-generated charges.

Different from combining PBA with semiconductor materials directly, Liu synthesized g-C_3N_4–Fe_2N composites with PB-derived Fe_2N and g-C_3N_4 through an electrostatic self-assembly method (Fig. 10).[103] The presence of Fe_2N could ameliorate the light absorption capacity, increase the electron–hole separation and facilitate the photo-electron transfer efficiency of the g-C_3N_4–Fe_2N composites in the visible-light region. However, the g-C_3N_4–Fe_2N composite exhibited a relatively poor photocatalytic H_2-generation rate of 88.7 μmol g^{-1} h^{-1}.

Graphdiyne (GDY) is a novel type of carbon-based material. Due to its special electronic structure and excellent semiconductor properties similar to silicon, GDY has been applied in photocatalytic reactions. Jin and Wang synthesized a $NiCo_2O_4$@GDY p–n heterojunction with PBA-derived hollow $NiCo_2O_4$ and GDY *via* the wet ball milling method (Fig. 11).[104] $NiCo_2O_4$@GDY showed 4.84 and 6.91 times the photocatalytic hydrogen performance (4.84 mmol g^{-1} h^{-1}) of single GDY and $NiCo_2O_4$, respectively. *In situ*-irradiated X-ray photoelectron

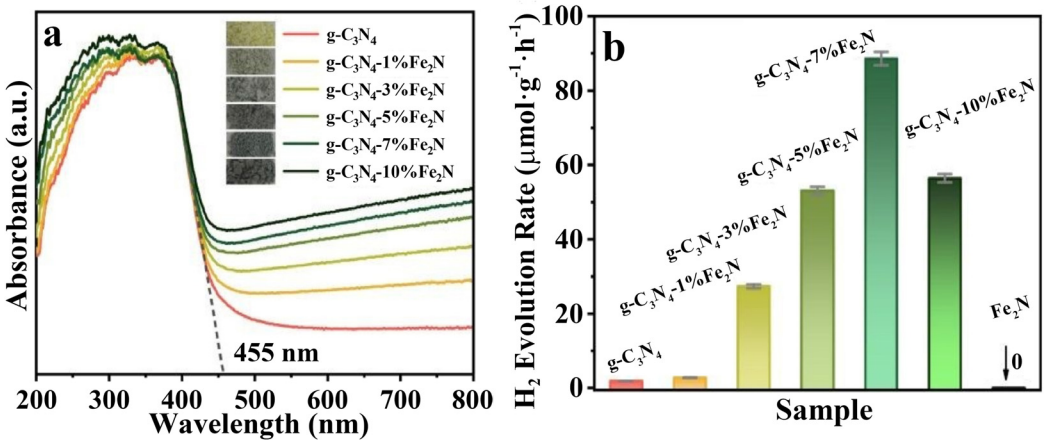

Fig. 10 (a) UV-vis absorption spectra of pure g-C_3N_4 and different g-C_3N_4–Fe_2N nanocomposites. (b) Average rates of H_2 evolution of pure g-C_3N_4 and different g-C_3N_4–Fe_2N nanocomposites under visible-light. Reproduced with permission from ref. 103. Copyright 2019, The Royal Society of Chemistry.

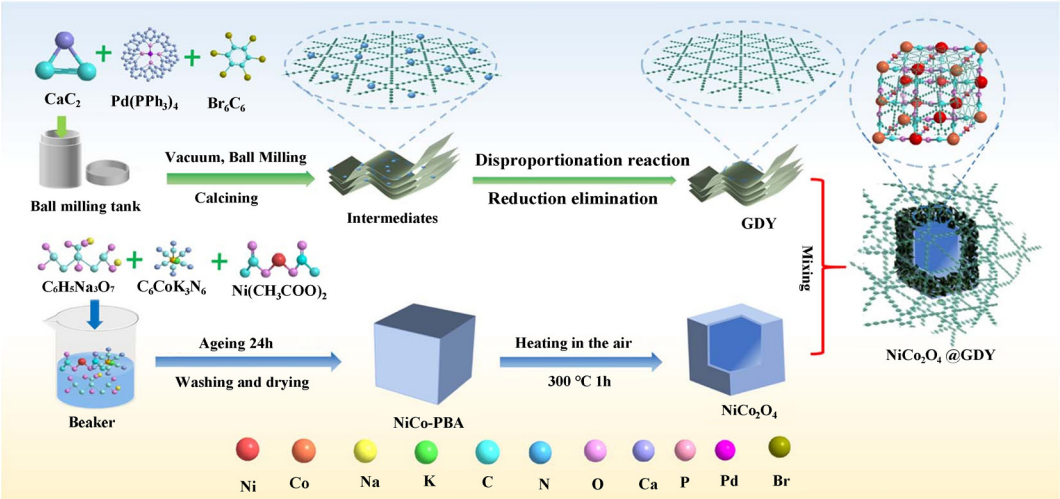

Fig. 11 Proposed synthesis process of $NiCo_2O_4$@GDY. Reproduced with permission from ref. 104. Copyright 2023, The Royal Society of Chemistry.

spectroscopy (ISI-XPS) analyses suggested that the excited electrons on $NiCo_2O_4$ can be transferred across its internal electric field to GDY in this tight p–n heterojunction, leading to the better separation of charge carriers.

In 2021, Lan and Chen prepared a Co–Co PBA/CdS composite (PB–Co/CdS–LT-*x*) with a beaded structure by integrating Co–Co PBA with CdS through the facile temperate-induced self-assembly method (Fig. 12).[106] PB–Co/CdS-LT-3 revealed high activity of 57.23 mmol g^{-1} h^{-1}. The DFT calculation analyses demonstrated that the strong coordination link between the Cd and –CN groups could deliver the photo-electrons between CdS nanowires and Co–Co PBA. Besides, the Co site may be the active center for hydrogen evolution. The theoretical calculation and Bader charge analysis indicated that the charges are transferred from CdS to Co–Co PBA and the photocatalytic H_2 evolution occurs on Co–Co PBA. This work validates the significance of coordination links in hybrid materials and provides a theoretical basis for the fabrication of beaded

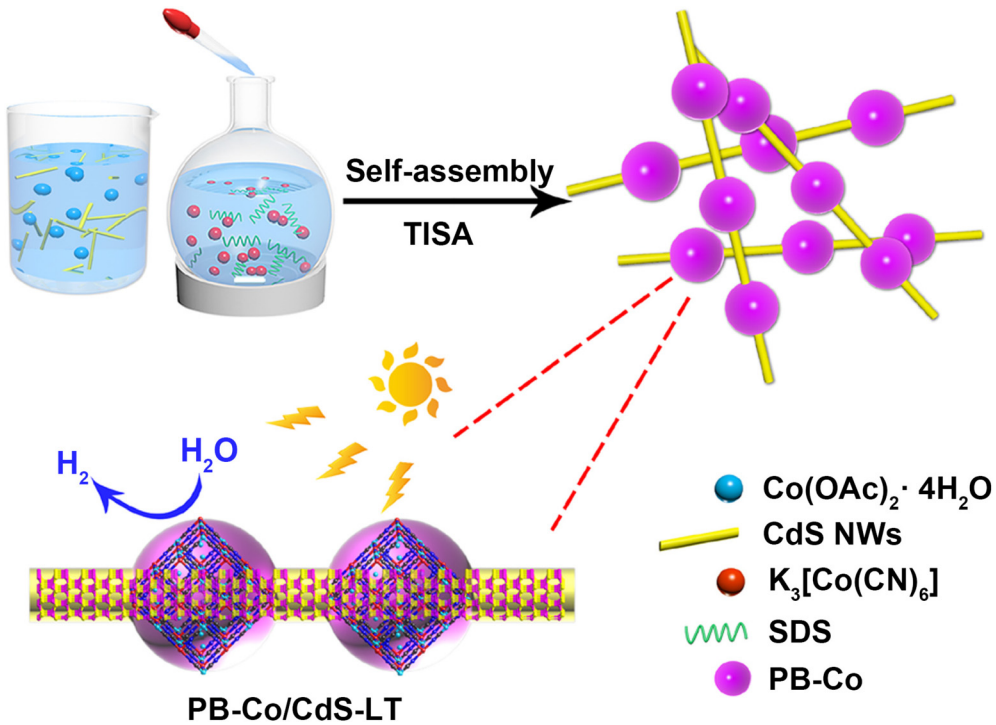

Fig. 12 Schematic illustration of the formation of PB–Co/CdS with a beaded structure and its application in photocatalytic H_2 evolution. Reproduced with permission from ref. 106. Copyright 2021, the American Chemical Society.

photocatalysts and porous coordination polymer composites. Similarly, Jin and Guo designed an S-Scheme heterojunction (CdS/ZnCdPBA-*x*) with CdS nanorods and Zn–Cd PBA in 2023.[107] The photocatalytic activity of the CdS/ZnCdPBA-15 composite (19.24 mmol g^{-1} h^{-1}) was lower than that of PB–Co/CdS–LT-3 under the same test conditions. In this work, the CdS/ZnCdPBA composite was constructed by electrostatic interactions, which promoted the charge transfer to a certain extent. In contrast, the coordination interactions may play a better role in accelerating the charge transfer. That is why the beaded structure Co–Co PBA/CdS showed a better photocatalytic performance.

In 2022, Jin designed a particular S-scheme heterostructure, ZnCdS/NiCoP, by assembling a Zn–Cd PBA-derived sulfide on Ni–Co PBA-derived phosphide.[108] ZnCdS/NiCoP-3% achieved an H_2 generation rate of 11.66 mmol g^{-1} h^{-1}, and the hydrogen production rate of this catalyst could be maintained at 80% after four cycles. The construction of an S-scheme heterojunction restrains the fast recombination of photo-electrons and holes, leading to a high H_2 evolution rate. In the same year, Tsubaki and Jin designed a novel photocatalysts, H–NCP/H–ZCS, by combining cubic-like ZnCdS (H–ZCS) with NiCoP frameworks (H–NPC), reaching a high H_2 generation rate of 73.00 mmol g^{-1} h^{-1}.[109] It is worth mentioning that H–NCP/H–ZCS has the highest hydrogen evolution rate among all PBA-derived photocatalysts reported thus far. H–NCP/H–ZCS possessed a double-hollow structure, which can enhance the diffusion, penetration, and mass transmission of the reaction species. At the same time, the migration distance of photogenerated charges in H–NCP/H–ZCS can be extremely shortened. These advantages endowed the catalyst with superstrong catalytic activity. In the same year, Yue and Yi designed a $ZnIn_2S_4$/CdS nanohybrid (ZIS/CS) by integrating ultrathin $ZnIn_2S_4$ nanosheets on the surface of hollow CdS cubes to form a cube-in-cube structure.[110] Firstly, the hollow CdS cubes were prepared using a Cd–Co PBA through a mild sulfuration condition. The first etching reagent was TAA and ammonia. At this time, the Co atoms in the Cd–Co PBA were removed, leaving crevices and forming a hollow structure. Then, the Na_2S further etched the precursor, constructing a core–shell structure CdS cube. Finally, $ZnIn_2S_4$ *in situ* grew on the surface of the hollow CdS cube through a hydrothermal reaction at 80 °C. When the amount of ZIS reached 30%, the 30% ZIS/CS exhibited the highest H_2 evolution rate of 7.4 mmol g^{-1} h^{-1}. The EPR, XPS and DFT analyses indicated that the electron transfer direction is from ZIS to CS, which may result in interfacial band bending, creating a Z-scheme charge transfer pathway in ZIS/CS.

Inspired by the above-mentioned strategies, Ding and Wang designed a PBA-derived type II p–n heterojunction, which was prepared by n-type CdS and p-type NiS.[111] Firstly, a small-sheet-structure CdS was grown on the Ni–Co PBA to form a type I heterojunction, CdS/Ni–Co PBA (CP). Then, an NiS/CdS (CN) catalyst was obtained with Na_2SO_3/Na_2S solution as the etching agent. The etching chemical equation is $Ni_3[Co(CN)_6]_2$ + S^{2-} (from Na_2S) → 3NiS + 2Co$[(CN)_6]^{3-}$. In the LA solution, the hydrogen evolution rate of CN-2 (the mass ratio of CdS was 73.9%) was greater than 66.3 mmol g^{-1} h^{-1}, which was 39 times higher than single CdS. In the LA solution, the charge transfer mechanism of CP-2 (the mass ratio of CdS is 56%) photocatalyst followed the typical type I heterojunction according to its band structures. The reduction reaction of protons and the consumption of holes will occur on Ni–Co PBA simultaneously. However, this route will give rise to the temporary separation of photo-generated electrons and holes, resulting in poor photocatalytic HER activity. Alternatively, in the CN-2 photocatalyst, the n-type CdS and p-type NiS may build a p–n heterojunction, which causing the mechanism to change from type I to type II. Based on the built-in electric field in the CN-2, the electrons will transfer from the CB of NiS to the CB of CdS and the holes of CdS may be delivered to the VB of NiS, leading to a better and faster charge transfer efficiency. This work provides a common strategy for boosting the photocatalytic performance of photocatalysts by the construction of a built-in electric field, paving a new way for the design of novel PBA-derived photocatalysts.

In conclusion, PBAs are fascinating precursors for the design of composite photocatalysts for photocatalytic H_2 evolution. PBA-derived materials with a hollow structure are a class of photocatalysts with the highest capacity for photocatalytic hydrogen production. However, the photocatalytic hydrogen production performance of the composite catalysts constructed by the direct combination of PBA and g-C_3N_4 or TiO_2 is far from satisfactory. In this case, designing and synthesizing complexes with new semiconductors (MOFs, COFs, *etc.*) and PBA-derived materials, forming strong interactions between the host and guest (coordination links between CdS and Co–Co PBA inref. 106), may be a new method to improve the catalytic performance of composite materials.

3.2. PBAs and their derived materials for photocatalytic water oxidation

PBAs are a type of reliable water-oxidation catalysts (WOCs) in both electrocatalytic and photocatalytic water oxidation.[112] PB has been applied with Ru-based photosensitizers for light-driven water oxidation reactions since 1985.[113] Different from photocatalytic H_2 evolution systems, PB can drive visible-light-driven water oxidation without Pt or sulfide. In water-oxidation reactions, PB acts as a catalyst rather than a REDOX medium. Thus, PBAs and their derived material have become the frontier of research in the last ten years. A variety of PBA-derived materials has been synthesized and applied in oxygen evolution for light-driven water splitting (a summary of different PBA-based photocatalysts for water oxidation is presented in Table 2). In this part, we summarize the application of water oxidation photocatalysts of PBAs by the following classification, PBAs, PBA-derived materials, and PBA-derived composites.

3.2.1. PBAs and their derived photocatalysts for water oxidation reaction. In 2014, PB, Mn–Fe PBA, Co–Fe PBA, Ni–Fe PBA, and Cu–Fe PBA were used as WOCs to drive water oxidation with a photosensitizer ($[Ru(bpy)_3]^{2+}$) and $Na_2S_2O_8$ at pH

Table 2 Summary of different PBA-based photocatalysts for water oxidation

Material	Irradiation	Sacrificial agent	Oxygen evolution rate	Photosensitizer	Ref.
PB	$\lambda > 360$ nm	$Na_2SO_4/Na_2S_2O_8$	1.5×10^{-4} mol dm^{-3}	RuBpy	113
Co–Co PBA	$\lambda > 470$ nm	$Na_2S_2O_8$	TOF = 2.7×10^{-4} s^{-1}	RuBpy	114
Co–Pt PBA	$\lambda > 420$ nm	$Na_2S_2O_8$	3712 μmol g^{-1} (5 min)	RuBpy	115
$Ca_x[Co^{II}(H_2O)_2]_{1.5-x}[Co^{III}(CN)_6]$	$\lambda > 420$ nm	$Na_2S_2O_8$	62 500 μmol g^{-1} (5 min)	RuBpy	116
CoFe@CoCo	$\lambda = 450$ nm	$Na_2S_2O_8$	2050 μmol g^{-1} h^{-1} (2 h)	RuBpy	117
[Ru–P_4VP–CoFe]	$\lambda > 420$ nm	$Na_2S_2O_8$	TOF = 5.6×10^{-4} s^{-1}	None	118
[Cobpy–Fe]	$\lambda = 475$ nm	$Na_2S_2O_8$	1594 μmol g^{-1} h^{-1} (1 h)	None	119
[Cophen–Fe]	$\lambda = 475$ nm	$Na_2S_2O_8$	1553 μmol g^{-1} h^{-1} (1 h)	None	119
[CoFe–MB]	$\lambda > 420$ nm	$Na_2S_2O_8$	71.3 μmol g^{-1} h^{-1} (2 h)	None	120
[CoFe–CM]	$\lambda > 420$ nm	$Na_2S_2O_8$	49.5 μmol g^{-1} h^{-1} (2 h)	None	120
[CoFe–SF]	$\lambda > 420$ nm	$Na_2S_2O_8$	28.4 μmol g^{-1} h^{-1} (2 h)	None	120
$Co_xFe_{3-x}O_4$	$\lambda > 420$ nm	$Na_2S_2O_8$	1900 μmol g^{-1} h^{-1} (13 min)	RuBpy	121
$Co_xFe_{3-x}O_4$	$\lambda > 420$ nm	$Na_2S_2O_8$	8500 μmol g^{-1} h^{-1} (13 min)	CAN	121
CoP/NC	$\lambda > 420$ nm	$Na_2S_2O_8$	3000 μmol g^{-1} (2 min)	RuBpy	122
Co_3O_4/NC	$\lambda > 420$ nm	$Na_2S_2O_8$	2000 μmol g^{-1} (2 min)	RuBpy	122
CoS_2/NC	$\lambda > 420$ nm	$Na_2S_2O_8$	1356 μmol g^{-1} (2 min)	RuBpy	122
$Cu(OH)_2$/CuO	$\lambda > 420$ nm	$Na_2S_2O_8$/NaOH	3567 μmol g^{-1} h^{-1} (6 h)	None	123
PB/b-TiO_2	$\lambda > 415$ nm	$Na_2S_2O_8$	1319 μmol g^{-1} h^{-1} (2 h)	None	124
LDH–PB-1	$\lambda > 420$ nm	$Na_2S_2O_8$	1830 μmol g^{-1} h^{-1} (2 h)	None	125
Niobate/PB	$\lambda > 350$ nm	$Na_2S_2O_8$	89.5 μmol g^{-1} h^{-1} (3 h)	None	126
Fe–Co PBA@ $BiVO_4$	$\lambda = 420$ nm	$NaIO_3$	2370 μmol g^{-1} h^{-1} (4 h)	None	127

= 7.[114] Co–Fe PBA maintained a faster oxygen production rate, whereas Mn–Fe PBA showed a lower activity and the other PBAs were all inactive. In contrast to using Fe as the cyanide center, metal Co has been introduced as the center of the cyanide, and Fe–Co PBA, Co–Co PBA and Mn–Co PBA have been synthesized and applied in photocatalytic water oxidation. Obviously, the reaction rate of Co–Co PBA was the highest, indicating that Co is an excellent active site for photocatalytic water oxidation. It is worth mentioning that the activity of Co_3O_4 cannot catch up with that of Co–Co PBA, proving the potential value of Co–Co PBA in WOC applications.

Fukuzumi and Yamada designed two PBA photocatalysts for photocatalytic water oxidation.[115,116] One is the Co–Pt PBA with different valences of Pt, and the other is Ca ion-incorporated Co–Co PBA. The stability of Co–Pt PBA was excellent, where it could maintain above 90% yield of O_2 in three cycles. The Ca ion-incorporated Co–Co PBA could afford O_2 with 200% quantum efficiency, reaching a high conversion efficiency of solar energy (Fig. 13). However, although PBAs can provide water oxidation activity, the light poisoning effect of the RuBpy photosensitizer in this type of photocatalytic system will restrain their wide application in photocatalytic water oxidations.

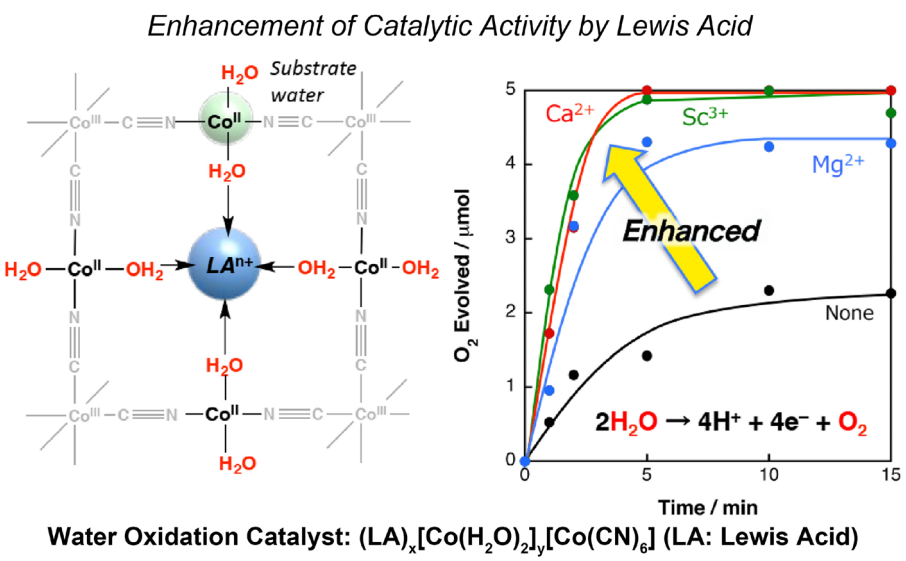

Fig. 13 Incorporation of a small amount of Ca^{2+} ions in a polymeric Co cyanide complex with enhanced activity for photocatalytic water oxidation. Reproduced with permission from ref. 116. Copyright 2017, The Royal Society of Chemistry.

The modification of PBA structures with a photosensitizer can effectively improve their catalytic stability in oxygen evolution. In 2018, Karadas, Yaglioglu and Dede prepared a [CoFe–TPyP] by connecting porphyrins as a photosensitizer on Co–Fe PBA.[117] [CoFe–TPyP] was used for photocatalytic water oxidation in a $K_2S_2O_8$ solution without the RuBpy photosensitizer. It could maintain good photocatalytic activity after three cycles within three hours. DFT calculations suggested that the Fe centers can donate electrons to the porphyrin, which may reduce the possibility of photo-electron and hole recombination, allowing the excited state to survive long enough for subsequent oxygen evolution reactions. This study demonstrates that combining PBA with photosensitive groups is an effective means to maintain the O_2 evolution rates. In the same year, to solve the problem of light poisoning, Karadas proposed a new photosensitizer catalyst (PS–WOC) with Co–Fe PBA and [Ru–P_4VP].[118] The oxidation state of the Ru site for [Ru–P_4VP–CoFe] is similar to RuBpy. Compared with driving water oxidation by PBAs and RuBpy, [Ru–P_4VP–CoFe] maintained its stability longer and demonstrated higher activity for photocatalytic water oxidation. The TOF of [Ru–P_4VP–CoFe] is 6×10^{-4} s^{-1}. The chemical bonding strategy between the catalyst and photosensitive groups can effectively alleviate the light poisoning issues in WOCs. In 2022, the Karadas group also reported a series of PS–WOCs by combining different photosensitive groups (PSs) with Co–Fe PBA.[119,120] A series of PSs including 1,10-phenanthroline (phen), coumarin (CM), safranin O (SF), and methylene blue (MB) was used to obtain different PS–WOCs, namely [Cophen$_2$–Fe], [CoFe–CM], [CoFe–SF] and [CoFe–MB], respectively. Compared with [Cophen$_2$–Fe], the [CoFe–PS] (PS = CM, SF and MB) catalysts exhibited better catalytic stability in 6 h. The highest O_2 evolution rate of 71.3 μmol g^{-1} h^{-1} was driven by [CoFe–MB] without RuBpy. The results in these studies show that PSs have different absorption bands and energy levels with a narrow HOMO–LUMO gap. The "plug and play" synthetic strategy of building PS–WOCs provides an ideal pathway to obtain efficient WOCs for photocatalytic reactions.

Iron-based metal oxides are good WOCs with a low cost, low toxicity, and rich REDOX properties. In 2015, Ding synthesized a series of PBA-derived materials, $M_xFe_{3-x}O_4$ (M = Fe, Co, Ni), using PBAs as a precursor by thermal decomposition.[121] In an $Na_2S_2O_8$ and RuBpy solution, the yield of O_2 for $Co_xFe_{3-x}O_4$ was 1900 μmol g^{-1} in 13 min, which was higher than that of $Ni_xFe_{3-x}O_4$ (1280 μmol g^{-1}) and Fe_2O_3 (460 μmol g^{-1}). The porous metal–oxide catalysts in the above-mentioned systems have weak catalytic stabilities, which produced almost no oxygen after 13 min. In contrast, in a ceric ammonium nitrate (CAN) solution, $Co_xFe_{3-x}O_4$ catalysts afforded a higher O_2 evolution rate of 8500 μmol g^{-1} in 45 min, which was also higher than that of $Ni_xFe_{3-x}O_4$ and Fe_2O_3. Meanwhile, the photocatalytic stability showed an obvious improvement in CAN solution, indicating that CAN is an excellent photosensitizer and sacrificial agent for photocatalytic water oxidation. In this work, the porous PBA-derived $Co_xFe_{3-x}O_4$ material is easily accessible, which may be applied commercially on a large scale.

In 2020, Ding prepared three Co–Co PBA-derived materials through high-temperature pyrolysis strategies, including CoP/NC, Co_3O_4/NC and CoS_2/NC.[122] The rate of O_2 evolution for the CoP/NC catalyst was 3000 μmol g^{-1} after 2 min photoirradiation, which is larger than that of Co_3O_4/NC (2000 μmol g^{-1}) and CoS_2/NC (1360 μmol g^{-1}). This study manifested that metal phosphides may be good WOCs, and the strategy of using PBA as a template to create metal phosphides may be a good way to explore high-stability and highly efficient WOCs.

3.2.2. PBA-derived composite photocatalysts for water-oxidation reaction. Similar to catalysts applied in photocatalytic hydrogen evolution, WOCs composed of PBA-derived composites have also been widely reported. In 2018, Wang designed $Co(OH)_2$/CuO nanoparticles using Cu–Co PBA as a precursor (Fig. 14).[123] In NaOH and $Na_2S_2O_8$ solutions, the $Co(OH)_2$/CuO nanoparticles displayed high catalytic efficiency (3567 μmol g^{-1} h^{-1}) in the visible-light-driven water oxidation reaction without the RuBpy photosensitizer. This work indicated that the $Co(OH)_2$/CuO nanoparticles could serve as both water oxi-

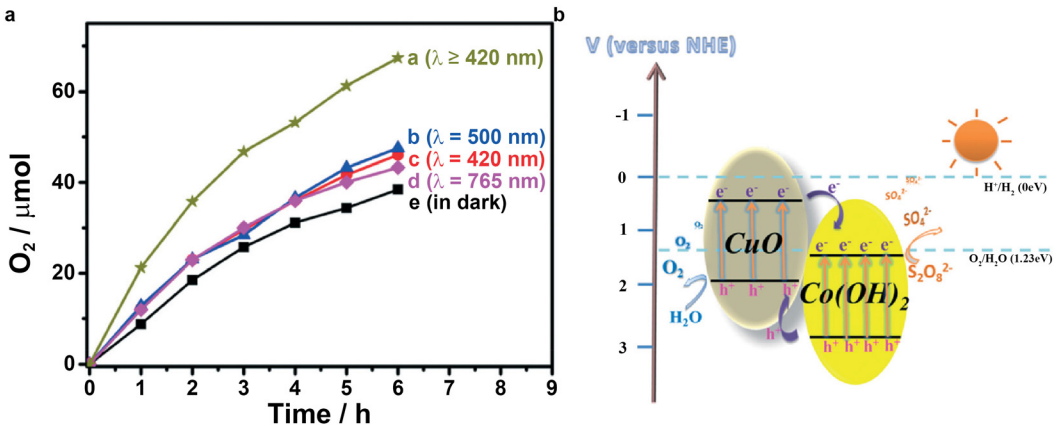

Fig. 14 (a) Examination for the photocatalytic activity of $Co(OH)_2$/CuO at different light wavelengths. (b) Schematic diagram of the band structure and charge transfer route for $Co(OH)_2$/CuO. Reproduced with permission from ref. 123. Copyright 2018, The Royal Society of Chemistry.

dation catalysts and visible light absorption centers. Also, the $Co(OH)_2$/CuO nanoparticles showed high stability in the reaction system. The synergistic effect between these two components was shown to be the key to the excellent photocatalytic activity in the water oxidation reaction process.

In 2020, Karadas designed PB/b-TiO_2 catalysts by *in situ* growing PB on b-TiO_2 (Fig. 15).[124] PB/b-TiO_2 exhibited remarkable photocatalytic oxidation activity compared to single b-TiO_2 and PB/TiO_2. The O_2 evolution rate of PB/b-TiO_2 reached 35.6 μmol h^{-1} with $Na_2S_2O_8$ as a sacrificial agent. Compared with TiO_2, the brown b-TiO_2 has a narrower band gap (1.95 eV) and more efficient absorption capacity, resulting in better activity for photocatalytic water oxidation. In the same year, this group prepared an LDH–PBA composite using ZnCr–LDH and Co–Fe PBA.[125] LDH–PBA exhibited a three-fold increase in activity (1.83 mmol g^{-1} h^{-1}) compared to single ZnCr–LDH and maintained better stability in 3 cycles. The transfer direction of the holes in the LDH–PBA composite was from ZnCr–LDH to Co–Fe PBA, which may give the LDH–PBA composite better photocatalytic ability compared with the single ZnCr–LDH. In 2021, Karadas and Unal designed a p–n junction using Co–Fe PBA and niobate ($Ca_2Nb_3O_{10}^-$) nanosheet through an *in situ* self-assembly strategy.[126] The niobate/PBA junction achieved an O_2 evolution rate of 48.6 μmol g^{-1} h^{-1} with $Na_2S_2O_8$ as a sacrificial agent, which was twice that of the single niobate nanosheets. Meanwhile, niobate/PBA exhibited good stability during a 12 h experiment for 4 cycles. The inverted-V-shaped Mott–Schottky curve of niobate/PBA indicated that a p–n junction was formed, constructing a built-in electric field and accelerating the transfer efficiency of the holes. This work suggests that building a p–n junction is an ideal method to prepare PBA-derived materials with improved catalytic activity for photocatalytic water oxidation.

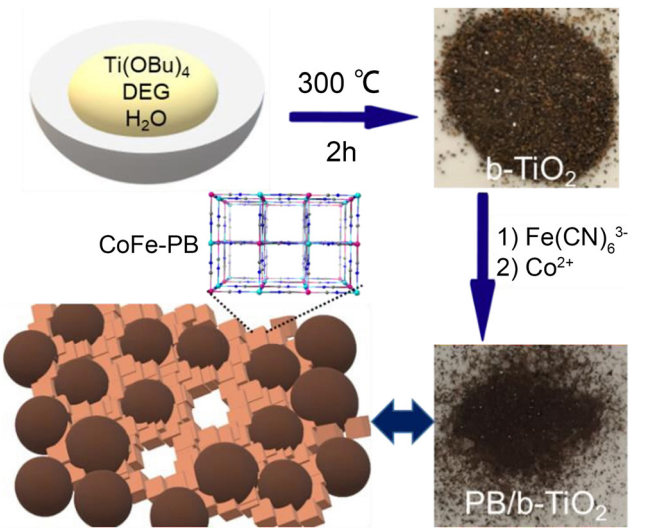

Fig. 15 Synthesis of PB/b-TiO_2 by incorporating Prussian blue in brown TiO_2 assemblies. Reproduced with permission from ref. 124. Copyright 2020, The Royal Society of Chemistry.

In 2023, Ding designed a series of PBA@$BiVO_4$ photocatalysts. Six types of M–Co PBA (M = Fe, Co, Ni, Cu, Zn and Mn) cocatalysts were deposited on the surface of $BiVO_4$.[127] The experimental data showed that coupling $BiVO_4$ with Co–Co PBA resulted in better light harvest ability compared to pure $BiVO_4$. Among the composite catalysts, Fe–Co PBA@$BiVO_4$ displayed the best activity for water oxidation with the O_2 evolution rate of about 2370 μmol g^{-1} h^{-1} in the presence of $NaIO_3$ as a sacrificial agent. This work indicates that the formation of composites facilitates the transfer of photogenerated charge carriers between the two components, meanwhile boosting the surface catalytic efficiency of $BiVO_4$.

Based on the studies discussed above, we can draw the following conclusions: PBAs have already been extensively applied in the field of light-driven water oxidation. In the initial report, PBAs were usually used with RuBpy and $Na_2S_2O_8$ as a photosensitizer and sacrificial reagent, respectively. Co-based PBAs possess the best photocatalytic activity for light-driven water oxidation. However, the light poisoning of RuBpy in these systems results in poor catalytic stability. The strategy of combining PBAs with photosensitizers not only results in enhanced photocatalytic activity, but also solves the problem of low catalytic stability caused by RuBpy photo-poisoning. Meanwhile, PBA-derived catalysts such as PBA-derived sulfides and phosphates can also improve the photocatalytic performance of water oxidation. Finally, loading PBAs on other semiconductor materials is an excellent modification method for constructing different heterogeneous structures. The formation of different heterojunctions can promote the charge transfer in WOCs, thereby enhancing the photocatalytic performance of PBA-derived WOCs.

3.3. PBAs and PBA-derived materials for CO_2 photoreduction

Compared with the photocatalytic hydrogen evolution and photocatalytic water oxidation reactions, the research on PBAs and PBA-derived materials for photocatalytic CO_2 reduction reaction (CO_2RR) is relatively less. Converting CO_2 into valuable chemicals has been regarded as the most effective way to promote the reuse of greenhouse gases. The current research on the use of PBAs and PBA-derived materials for photocatalytic CO_2RR are mainly carried out in two systems, as follows: system I "CO_2 + H_2O" and system II "CO_2 + H_2". System I can be described as follows: this type of photocatalytic CO_2RR process usually takes place in aqueous solution. CO_2 and H_2O are applied as reactants to generate CO and H_2, respectively, or some other alkyl compounds (CH_4, HCOOH, HCHO, *etc.*). System II can be described as follows: a "CO_2 + H_2" gas mixture is used as the reactant to achieve the conversion of carbon to CO and H_2O or some other alkyl compounds (CH_4, HCOOH, HCHO, *etc.*). This technology is the reverse reaction of water gas shift (RWGS).

The selectivity and CO_2 conversion rate are the main parameters to evaluate the photocatalytic ability of a CO_2RR catalyst. Metal or mixed-metal oxides and metal sulfides are fascinating catalysts for photocatalytic CO_2RR.[128–131] The characteristics of PBA materials can improve the performance of cata-

lysts in these two evaluation systems. The advantages of PBAs for photocatalytic CO_2RR are as follows: (i) PBAs have intrinsic micropores structures, which are large enough for CO_2 molecules to access. Furthermore, the N atoms in their structure can interact with CO_2 molecules, endowing PBAs with good affinity for carbon dioxide. (ii) The synergistic effect between the bimetals in PBAs can enhance the photocatalytic activity and selectivity for CO_2RR. (iii) Owing to the tiny pores inside PBAs, the force between N atoms and adsorbed CO_2 molecules can assist CO_2 getting closer to the active sites of the metal, promoting the photocatalytic reaction. (iv) PBAs have fascinating stability and adjustable structures. Therefore, in conclusion, these superiorities will make PBA a good candidate for photocatalytic CO_2 photoreduction.

3.3.1. PBA-derived photocatalysts for CO_2 photoreduction reactions. As long ago as 2012, Karadas found that M_1–M_2 PBAs (M_1 = Mn, Fe, Co, Ni, Cu; M_2 = Fe, Co) have fascinating CO_2 adsorption capacities.[132] When M_1 is Cu or Co, PBAs can absorb more CO_2 gas. This property endows PBAs with good potential in CO_2 photoreduction. To further explore PBA-based photocatalysts for CO_2 photoreduction, a few PBA-derived photocatalysts with different structures has been reported in recent years (a summary of different PBA-based photocatalysts for CO_2RR is shown in Table 3).

In 2019, Lou prepared a PBA-derived colloidal cluster (CC) having enhanced catalytic activity for CO_2 photoreduction.[133] The Co–Fe PBA CC was constructed by 8 smaller Co–Fe PBA nanoparticles (NPs) and there was a void space in Co–Fe PBA CC, forming a zeolite structure. The formation process is as follows: small PBA nanocubes with truncated corners were obtained firstly, and then eight satellites grew on their corners, and then grew larger. They orderly got closer along the edges of the cores, and then attached to form cubic architectures by taking advantage of the anchoring effect supplied from the cores. At the same time, the cores in the PBA NPs were completely removed, transforming the core@satellite structure into an open Co–Fe PBA CC (Fig. 16). This marvelous structure enabled the Co–Fe PBA CC to achieve a high CO production rate of 11.7 mmol h^{-1} g^{-1} (in system I) and high selectivity of 77.5%. Meanwhile, the co-product was just H_2 without other hydrocarbon products.

In 2021, Ding prepared a series of PBAs (M_{II}–M_{III} PBAs, M_{II} = Mn, Fe, Co, Ni and Cu; M_{III} = Fe or Co) to drive CO_2 photoreduction reaction with RuBpy and TEOA in an aqueous solution of acetonitrile.[134] In this system (system I), there were only two types of products, *i.e.*, H_2 and CO. Ni–Co PBA exhibited a better photocatalytic CO_2 conversion performance. The CO evolution rate of Ni–Co PBA was 140 mmol g^{-1} h^{-1} (with 0.5 mg catalyst) and the selectivity of Ni–Co PBA reached 96.8% (with 0.25 mg catalyst). The H_2 adsorption and desorption experiments suggested that the photocatalytic CO_2RR activities of M_{II}–Co PBAs are better than that of M_{II}–Fe PBAs, but the M_{II}–Fe PBAs have better selectivity. The DFT analysis revealed that Ni–Co PBA has a lower energy barrier value around the transformation of absorbed $*CO_2$ to *COOH. At the same time, the Ni–Co PBA also has a lower energy barrier to absorb H* intermediates. Consequently, Ni–Co PBA exhibited a high CO_2 conversion efficiency and relatively low selectivity.

In 2022, Yan designed a series of FeNi-based metal/oxide composites and FeNi-based alloys by the hydrogen reduction method using Ni–Fe PBAs as the precursor.[135] When the reaction temperature was lower than 400 °C, Ni–Fe PBA was gradually transformed into a metal/oxide heterostructure. When the temperature reached 400 °C, the cyano group may disappear to form an $FeNi_3$ alloy. Thus, there are four product, namely NiFe-250, NiFe-300, NiFe-400 and NiFe-500, during the hydrogen reduction process at different temperatures. The CO_2 photoreduction test (in system II) results suggest that the reverse water–gas shift reaction and hydrogenation from CO_2 to CH_4 and C_{2-4} (two, three or four carbon hydrocarbons) hydrocarbons can be simultaneously promoted by the existence of NiFe-300 catalyst at different temperatures, achieving the excellent selectivity of 33.6% from CO_2 to C_{2-4}. The results of the *in situ* diffuse reflectance FT-IR spectroscopy measurements indicated that the formation of hydrocarbons may be caused by a two-step route of reverse water gas shift reaction and Fischer–Tropsch synthesis.

In 2023, Fang, Zhu and Li prepared an Ni–Fe–Co-based metal oxide (NCF–TMO) using Ni–Fe–Co PBA as the precursor at 400 °C.[136] NCF–TMO was formed by NiO, Co_3O_4, and Fe_2O_3 and achieved a high reaction rate (in system II) in the reduction of CO_2 to CO (2.9 mmol g^{-1} h^{-1}) and CH_4 (1.6 mmol g^{-1} h^{-1}). The mechanism analysis suggested that NCF–TMO has an efficient e–h separation ability under photothermal stimulation.

Table 3 Summary of different PBA-based photocatalysts for CO_2RR

Materials	Irradiation	Sacrificial agent	Main products	Productivity/(mmol h^{-1} g^{-1})	Selectivity/(%)	Ref.
Co–Fe PBA CC-1	$\lambda \geq 400$ nm	TEOA	CO	11.7	77.5	133
Ni–Co PBA	λ = 460 nm	TEOA	CO	140	96.8	134
NiFe-300	CEL-PF300-T3 Xe light	None	$CO/CH_4/C_{2-4}$	None	23.4/43.0/33.6	135
NCF–TMO	300 W Xenon lamp	None	CO/CH_4	2.9/1.6	None	136
Co^{III}–PBA@Co^{II}–PBA	$\lambda \geq 420$ nm	TEOA	CO/H_2	50.56	CO/H_2 = 1 : 1	137
$Ni(OH)_2$/PB	$\lambda \geq 420$ nm	TEOA	CO	108.8	88.2–95.0	138
Co–Co PBA/$CoSn(OH)_6$/Pt	$\lambda \geq 420$ nm	None	CO	0.0117	91.8	139
PW_{12}@Co	λ = 460 nm	TEOA	CO	0.75	90.7	140
PW_{12}@CoNi	λ = 460 nm	TEOA	CO	1.00	92.6	140

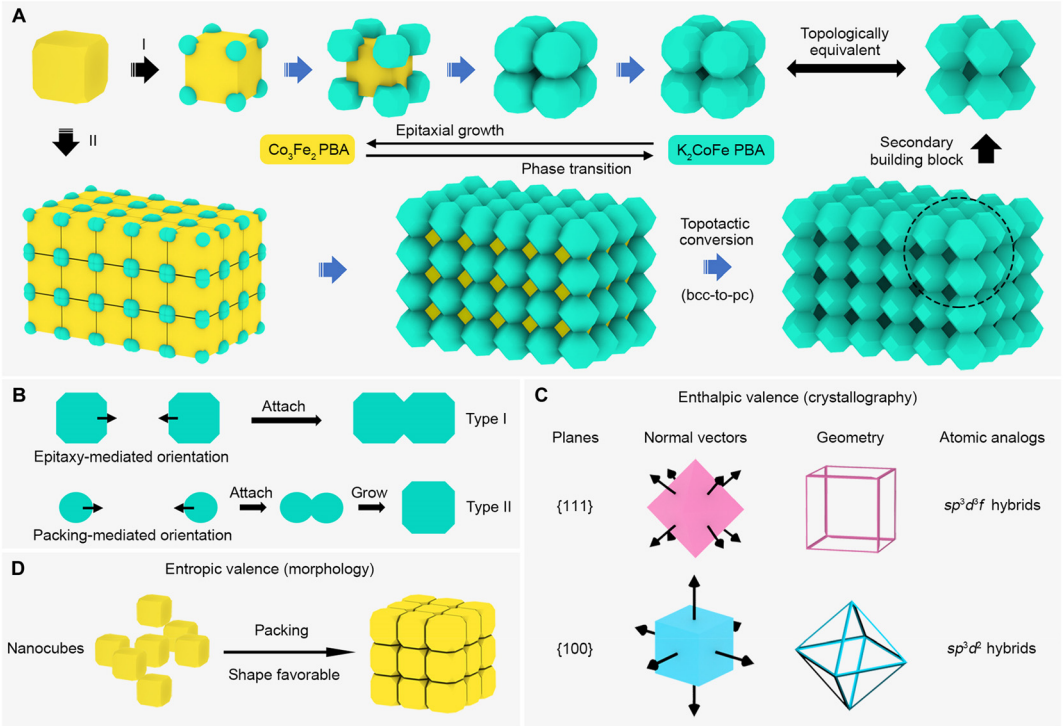

Fig. 16 (A) Schematic illustration of the formation routes of Co–Fe PBA CCs. (B) Two pathways toward the orientation of SNCs for the following attachment. (C) Illustration of the enthalpic valence of NCs and their atomic analogs. (D) Illustration of the entropic valence of NCs. Reproduced with permission from ref. 133. Copyright 2019, American Association for the Advancement of Science.

3.3.2. PBA-derived composite photocatalysts for CO_2 photoreduction reactions. In the above-mentioned descriptions, we concluded that PBAs and PBA-derived materials are excellent photocatalysts for CO_2 photoreduction. Also, using PBAs and their PBA-derived materials to construct a series of composite photocatalysts is also an efficient way to improve the catalytic performance for CO_2 photoreduction.

In 2022, two different studies on PBA-derived composite photocatalysts were reported by the Yu and Zhuang groups, respectively.[137,138] Firstly, a Co^{III}–PBA@Co^{II}–PBA heterojunction was obtained using two Co–Fe PBAs with different valence states. In this study, Co^{III}–PBA formed a cage outside Co^{II}–PBA, forming a core–shell structure. Due to the presence of Co^{III}/Co^{II}, the Co^{III}–PBA@Co^{II}–PBA achieved a high CO yield of 50 mmol g^{-1} h^{-1} (CO/H_2 = 1 : 1) in a TEOA and RuBpy solution (system I). The DFT calculations indicated that Co^{III}–PBA has a more negative CO_2 adsorption energy, endowing it with enhanced adsorption and activation ability for CO_2. Secondly, a series of Z-scheme $Ni(OH)_2$-*x*/PB (*x* = 1, 2, 4, 8, or 16) photocatalysts was prepared, which was formed by PB and $Ni(OH)_2$ nanosheets. The $Ni(OH)_2$-4/PB photocatalyst possessed a 1.5 nm atomic-level $Ni(OH)_2$ layer, which was vertically grown on PB. This special structure could expose more Ni sites on the surface of the catalyst. The XPS results, DFT calculations and EPR measurements indicated that the photo-generated electrons are transferred from PB to $Ni(OH)_2$, following the Z-scheme mechanism. $Ni(OH)_2$-4/PB exhibited a higher CO evolution rate of 108.8 mmol h^{-1} g^{-1} (with 0.05 mg catalyst) with a selectivity of 88.2% (system I). When 1 mg $Ni(OH)_2$-4/PB was added to the photocatalytic system, a low CO evolution rate (8.18 mmol h^{-1} g^{-1}) and high selectivity of 95% were obtained. This study proves that the construction of Z-scheme heterojunctions is an effective strategy to improve the catalytic performance of photocatalytic CO_2 reduction.

In the same year, Xiao prepared a Co–Co PBA/$CoSn(OH)_6$/Pt heterojunction using Co–Co PBA as a precursor.[139] In this work, $CoSn(OH)_6$ was *in situ* grown on the etched Co–Co PBA to form a Co–Co PBA/$CoSn(OH)_6$ precursor, and then Pt was deposited on the Co–Co PBA/$CoSn(OH)_6$ precursor under visible light to obtain a Co–Co PBA/$CoSn(OH)_6$/Pt heterojunction. The Co–Co PBA/$CoSn(OH)_6$/Pt heterojunction possessed a unique inlaid and hollow structure, which can increase the photocatalytic activity by multiple light scattering. The photocatalytic CO_2-to-CO rate of the Co–Co PBA/$CoSn(OH)_6$/Pt heterojunction reached 11.7 μmol g^{-1} h^{-1} with a high selectivity of 91.8% (system I). The by-product in this system was CH_4. This study proposes a collaborative surface regulation method to build PBA-derived composite photocatalysts. However, the photocatalytic performance of this Co–Co PBA/$CoSn(OH)_6$/Pt photocatalyst was less than satisfactory. In the following year, Wu *et al.* designed an Ni–Co PBA-derived PBA–S/PDI hybrid photocatalyst *via* a step-by-step strategy. The PBA–S/PDI hybrid photocatalyst showed higher CO_2-to-CO activity (15.0 μmol g^{-1} h^{-1}) than the Co–Co PBA/$CoSn(OH)_6$/Pt photocatalyst. The

PBA–S/PDI hybrid is an S-scheme heterojunction, which may result in a fast photo-electron migration process to drive photocatalytic CO_2RR. These studies suggest that constructing an S-scheme heterojunction is a successful strategy to boost the performance of photocatalytic CO_2RR.

Polyoxometallate (POM) has been widely used in photocatalytic CO_2RR because of its good stability and excellent REDOX property. In 2024, Ding designed two PBA-derived unique structures, namely PW_{12}@CoNi and PW_{12}@Co, *via* hydrothermal etching and annealing methods.[140] PW_{12}@CoNi and PW_{12}@Co possessed a hollow yolk–shell structure, which can expose more active sites for photocatalytic reaction. Compared with PW_{12}@Co, PW_{12}@CoNi had a relatively lower hydrogen desorption energy. This characteristic endowed PW_{12}@CoNi with stronger CO_2 adsorption ability, higher CO evolution rate (15.1 μmol g^{-1} h^{-1}) and higher selectivity (92.6%) in system I.

4. Conclusion and outlook

In this review, we discussed the recent developments, synthetic strategies and applications of PBA-derived materials in the field of photocatalytic H_2 evolution, photocatalytic O_2 evolution and photocatalytic CO_2 reduction. Although these photocatalytic reactions can help realize the conversion from solar energy to high value chemicals, due to their low activity, poor stability and low selectivity, there is still a long way to really apply these conversions on a large scale. Many strategies for structure modification and morphological adjustments have been discussed to improve the performance of PBA-derived photocatalysts. Sulfuration, phosphide and constructing composites are the most important methods for PBAs to become effective photocatalysts. To date, several common bottlenecks still exist in PBA-derived photocatalysts, and thus we also list some future directions at the end of this review.

(i) Most of the effective PBA-derived photocatalysts are PBA-derived sulfides or phosphides. The common synthesis methods always require substances containing sulfur or phosphorus, such Na_2S, TAA, phosphorus powder, and phosphate. However, all of them are toxic substances, which are harmful to the environment and human body. In the future, nontoxic organic sulfides and organic phosphides may be used to replace the above-mentioned substances to modify PBAs and their derived materials.

(ii) At present, most PBA-derived composites are constructed by molecule interactions or weak electrostatic interactions. The construction of PBA-derived composites through coordination bonds or covalent bonds can not only improve the stability of composite materials, but also provide a better platform for photo-electron migration, thus achieving rapid photo-electron hole separation and improving the photocatalytic performance of PBA-derived composites.

(iii) Constructing heterojunctions is an effective strategy to help electron transfer, promote the utilization of photo-generated electrons and get higher catalytic activities for PBA-derived materials. At present, type I heterojunctions, type II heterojunctions, S-scheme heterojunctions, Z-scheme heterojunctions, and p–n heterojunctions have been formed in PBA-derived photocatalysts. Generally, the formation of p–n heterojunctions is more beneficial to enhance the performance of PBA-derived photocatalysts.

(iv) PBAs and their derivatives are easy to synthesize, and the morphology, size and crystallinity of PBAs can be adjusted by synthetic method control. However, the nucleation and crystallization process of PBAs and PBA-derived materials are complicated due to their different nucleation rates and K_{sp} values. Thus, precise structure control of PBAs cannot be realized. Meanwhile, the photoelectron transfer path of PBA-derived photocatalysts has not been studied deeply. In further studies on PBA-derived photocatalysts, providing *in situ* characterization experiments and appropriate theoretical calculations is crucial in the design and preparation of high-efficient PBA-derived photocatalysts. Besides, combining theoretical calculations and *in situ* characterization experiments may help confirm the active sites, electron transfer directions and product formation process in photocatalytic reactions.

(v) The photocatalytic processes driven by PBAs and their derivatives generally need photosensitizers to surmount their problems of low light harvesting. In these photocatalytic reactions, EY and RuBpy are popular photosensitizers. However, these photosensitizers are very soluble in water, making them difficult to recycle. If these solutions are not properly treated and discharged into the environment, they will cause serious environmental pollution. In this case, connecting photosensitizers to photocatalysts can enable the recycle and reuse of photosensitizers. Although this type of strategy has been reported in recent years (WOCs), few researchers have applied it in the design of photocatalysts. In the future, we should focus on the design of photocatalysts combining PBA-derived materials and photosensitizers. Besides, there are no photosensitizers that can be used under acidic conditions. PBAs are extremely resistant to acid, and the design of new acid-resistant photosensitizers for PBAs can expand the application range of PBA-derived photocatalysts.

(vi) Cyanogen is a type of strong field ligand, in which both the C and N atoms can form coordination bonds with metal ions as coordination atoms to construct low-spin inner orbital coordination compounds, which have higher crystallinity and stability than bimetallic MOF materials (with carboxyl compounds as ligands). At present, the preparation of bimetallic MOF materials is relatively complex, and it is difficult to control the proportion of different metals. On the contrary, PBAs can precisely achieve metal regulation due to the fixed metal atomic ratio in PBAs.

(vii) Few PBAs and their derivatives can combine all their advantages such as facile preparation, low cost, excellent photocatalytic performance and high stability. In H_2 evolution reactions, most of PBA-derived photocatalysts cannot drive a higher reaction rate than 20 mmol g^{-1} h^{-1}. Also, in water oxidation reactions, most PBA-derived WOCs cannot be used for a long time. In photocatalytic CO_2RR, the selectivity of PBA-

derived photocatalysts is difficult to reach more than 95%. In the future, the construction of ternary or multi-component PBA-based photocatalysts is expected to achieve the goals of increasing the photocatalytic hydrogen evolution rate, boosting the catalytic stability for water oxidation and improving the selectivity for CO_2RR.

Conflicts of interest

There are no conflicts to declare.

Acknowledgements

This work was financially supported by the National Natural Science Foundation of China (No. 22271022 and 21701016), the Science and Technology Development Planning of Jilin Province (No. YDZJ202201ZYTS342). Partial support from the Robert A. Welch Foundation (B-0027) is also acknowledged (SM).

References

1 S. A. Hussain, F. Razi, K. Hewage and R. Sadiq, The perspective of energy poverty and 1st energy crisis of green transition, *Energy*, 2023, **275**, 127487–127496.
2 J. Li, S. Sun, D. Sharma, M. S. Ho and H. Liu, Tracking the drivers of global greenhouse gas emissions with spillover effects in the post-financial crisis era, *Energy Policy*, 2023, **174**, 113464–113478.
3 A. Hussain, S. M. Arif and M. Aslam, Emerging renewable and sustainable energy technologies: State of the art, *Renewable Sustainable Energy Rev.*, 2017, **71**, 12–28.
4 X. Chen, C. Li, M. Grätzel, R. Kostecki and S. S. Mao, Nanomaterials for renewable energy production and storage, *Chem. Soc. Rev.*, 2012, **41**, 7909–7937.
5 Z. Wang, C. Li and K. Domen, Recent developments in heterogeneous photocatalysts for solar-driven overall water splitting, *Chem. Soc. Rev.*, 2019, **48**, 2109–2125.
6 C. Zhao, Z. Chen, R. Shi, X. Yang and T. Zhang, Recent advances in conjugated polymers for visible–light–driven water splitting, *Adv. Mater.*, 2020, **32**, 1907296–1907248.
7 R. Pan, J. Liu and J. Zhang, Defect engineering in 2D photocatalytic materials for CO_2 reduction, *ChemNanoMat*, 2021, **7**, 737–747.
8 J. Yang, H. Bai, Y. Guo, H. Zhang, R. Jiang, B. Yang, J. Wang and J. C. Yu, Photodriven disproportionation of nitrogen and its change to reductive nitrogen photofixation, *Angew. Chem., Int. Ed.*, 2020, **60**, 927–936.
9 L. Jiao, J. Wang and H.-L. Jiang, Microenvironment modulation in metal-organic framework-based catalysis, *Acc. Mater. Res.*, 2021, **2**, 327–339.
10 M. Xia, X. Yan, H. Li, N. Wells and G. Yang, Well-designed efficient charge separation in 2D/2D doped $La_2Ti_2O_7$/$ZnIn_2S_4$ heterojunction through band structure/morphology reg N ulation synergistic effect, *Nano Energy*, 2020, **78**, 105401–105408.
11 H. Wang, H. Wang, Z. Wang, L. Tang, G. Zeng, P. Xu, M. Chen, T. Xiong, C. Zhou, X. Li, D. Huang, Y. Zhu, Z. Wang and J. Tang, Covalent organic framework photocatalysts: structures and applications, *Chem. Soc. Rev.*, 2020, **49**, 4135–4165.
12 K. Wenderich and G. Mul, Methods, mechanism, and applications of photodeposition in photocatalysis: A review, *Chem. Rev.*, 2016, **116**, 14587–14619.
13 T. Q. Trung and N. E. Lee, Recent progress on stretchable electronic devices with intrinsically stretchable components, *Adv. Mater.*, 2016, **29**, 1603167.
14 T. Watanabe, T. Takirawa and K. Honda, Photocatalysis through excitation of adsorbates. Rhodamine B adsorbed to CdS, *J. Phys. Chem.*, 1977, **81**, 1845–1851.
15 M. Halmann, Photoelectrochemical reduction of aqueous carbon dioxide on p-type gallium phosphide in liquid junction solar cells, *Nature*, 1978, **275**, 115–116.
16 H.-N. Wang, Y.-H. Zou, H.-X. Sun, Y. Chen, S.-L. Li and Y.-Q. Lan, Recent progress and perspectives in heterogeneous photocatalytic CO_2 reduction through a solid-gas mode, *Coord. Chem. Rev.*, 2021, **438**, 213906–213948.
17 D. Zhao and C.-F. Yang, Recent advances in the TiO_2/CdS nanocomposite used for photocatalytic hydrogen production and quantum-dot-sensitized solar cells, *Renewable Sustainable Energy Rev.*, 2016, **54**, 1048–1059.
18 Y. Yuan, R.-T. Guo, L.-F. Hong, X.-Y. Ji, Z.-D. Lin, Z.-S. Li and W.-G. Pan, A review of metal oxide-based Z-scheme heterojunction photocatalysts: actualities and developments, *Mater. Today Energy*, 2021, **21**, 100829–100867.
19 C. Liu, C. Kong, F.-J. Zhang, C.-M. Kai, W.-Q. Cai, X.-Y. Sun and W.-C. Oh, Research progress of defective MoS_2 for photocatalytic hydrogen evolution, *J. Korean Ceram. Soc.*, 2021, **58**, 135–147.
20 Y. Ren, D. Zeng and W.-J. Ong, Interfacial engineering of graphitic carbon nitride (g-C_3N_4)-based metal sulfide heterojunction photocatalysts for energy conversion: A review, *Chin. J. Catal.*, 2019, **40**, 289–319.
21 X. Zhang, X. Yuan, L. Jiang, J. Zhang, H. Yu, H. Wang and G. Zeng, Powerful combination of 2D g-C_3N_4 and 2D nanomaterials for photocatalysis: Recent advances, *Chem. Eng. J.*, 2020, **390**, 124475.
22 S. Liu, M. Wang, Y. He, Q. Cheng, T. Qian and C. Yan, Covalent organic frameworks towards photocatalytic applications: Design principles, achievements, and opportunities, *Coord. Chem. Rev.*, 2023, **475**, 214882–214918.
23 J.-E. Zhou, J. Chen, Y. Peng, Y. Zheng, A. Zeb and X. Lin, Metal-organic framework-derived transition metal sulfides and their composites for alkali-ion batteries: A review, *Coord. Chem. Rev.*, 2022, **472**, 214781–214813.
24 C. X. Chen, Y. Y. Xiong, X. Zhong, P. C. Lan, Z. W. Wei, H. Pan, P. Y. Su, Y. Song, Y. F. Chen, A. Nafady, S. Uddin and S. Ma, Enhancing Photocatalytic Hydrogen Production via the Construction of Robust Multivariate Ti–MOF/COF Composites, *Angew. Chem., Int. Ed.*, 2021, **61**, e202116874.

25 J. Jin, J. Yu, D. Guo, C. Cui and W. Ho, A hierarchical Z-scheme CdS-WO_3 photocatalyst with enhanced CO_2 reduction activity, *Small*, 2015, **11**, 5262–5271.
26 J. Shi, Z. Su, X. Li, J. Feng and C. Men, Impacts of host–guest assembly on the photophysical and photocatalytic properties of heterogenized molecular photosensitizer and catalysts, *J. Mater. Chem. A*, 2023, **11**, 6646–6658.
27 Y. Wang, H. Suzuki, J. Xie, O. Tomita, D. J. Martin, M. Higashi, D. Kong, R. Abe and J. Tang, Mimicking natural photosynthesis: Solar to renewable H_2 fuel synthesis by Z-scheme water splitting systems, *Chem. Rev.*, 2018, **118**, 5201–5241.
28 Q. Xu, L. Zhang, B. Cheng, J. Fan and J. Yu, S-scheme heterojunction photocatalyst, *Chem*, 2020, **6**, 1543–1559.
29 J. Low, J. Yu, M. Jaroniec, S. Wageh and A. A. Al-Ghamdi, Heterojunction photocatalysts, *Adv. Mater.*, 2017, **29**, 1601694.
30 H. Tada, T. Mitsui, T. Kiyonaga, T. Akita and K. Tanaka, All-solid-state Z-scheme in CdS-Au-TiO_2 three-component nanojunction system, *Nat. Mater.*, 2006, **5**, 782–786.
31 W. Tu, Y. Zhou, S. Feng, Q. Xu, P. Li, X. Wang, M. Xiao and Z. Zou, Hollow spheres consisting of $Ti_{0.91}O_2$/CdS nanohybrids for CO_2 photofixation, *Chem. Commun.*, 2015, **51**, 13354–13357.
32 K. Maeda, Z-scheme water splitting using two different semiconductor photocatalysts, *ACS Catal.*, 2013, **3**, 1486–1503.
33 J. Low, C. Jiang, B. Cheng, S. Wageh, A. A. Al-Ghamdi and J. Yu, A review of direct Z–scheme photocatalysts, *Small Methods*, 2017, **1**, 1700080–1700101.
34 N. Xiao, S. Li, X. Li, L. Ge, Y. Gao and N. Li, The roles and mechanism of cocatalysts in photocatalytic water splitting to produce hydrogen, *Chin. J. Catal.*, 2020, **41**, 642–671.
35 N. Zhang, S. Xie, B. Weng and Y.-J. Xu, Vertically aligned ZnO-Au@CdS core-shell nanorod arrays as an all-solid-state vectorial Z-scheme system for photocatalytic application, *J. Mater. Chem. A*, 2016, **4**, 18804–18814.
36 Z. Wang, X. Yue and Q. Xiang, MOFs-based S-scheme heterojunction photocatalysts, *Coord. Chem. Rev.*, 2024, **504**, 215674.
37 M. Chen, K. Umer, B. Li, Z. Li, K. Li, W. Sun and Y. Ding, Metalloporphyrin based MOF-545 coupled with solid solution $Zn_xCd_{1(-x}S$ for efficient photocatalytic hydrogen production, *J. Colloid Interface Sci.*, 2024, **653**, 380–389.
38 J. Qiu, K. Meng, Y. Zhang, B. Cheng, J. Zhang, L. Wang and J. Yu, COF/In_2S_3 S–scheme photocatalyst with enhanced light absorption and H_2O_2-production activity and fs–TA investigation, *Adv. Mater.*, 2024, 2400288, DOI: 10.1002/adma.202400288.
39 V. Soni, P. Singh, A. A. P. Khan, A. Singh, A. K. Nadda, C. M. Hussain, Q. Van Le, S. Rizevsky, V.-H. Nguyen and P. Raizada, Photocatalytic transition-metal-oxides-based p-n heterojunction materials: synthesis, sustainable energy and environmental applications, and perspectives, *J. Nanostruct. Chem.*, 2022, **13**, 129–166.
40 L. Che, J. Pan, K. Cai, Y. Cong and S.-W. Lv, The construction of p-n heterojunction for enhancing photocatalytic performance in environmental application: A review, *Sep. Purif. Technol.*, 2023, **315**, 123780.
41 Q. Wen, K. Yang, D. Huang, G. Cheng, X. Ai, Y. Liu, J. Fang, H. Li, L. Yu and T. Zhai, Schottky heterojunction nanosheet array achieving high–current–density oxygen evolution for industrial water splitting electrolyzers, *Adv. Energy Mater.*, 2021, **11**, 2102353–2102365.
42 S. Du, X. Lin, C. Li, G. Li, B. Zheng, Y. Liu, H. Xu and P. Fang, $CoSe_2$ modified Se-decorated CdS nanowire Schottky heterojunctions for highly efficient photocatalytic hydrogen evolution, *Chem. Eng. J.*, 2020, **389**, 124431.
43 L.-M. Cao, D. Lu, D.-C. Zhong and T.-B. Lu, Prussian blue analogues and their derived nanomaterials for electrocatalytic water splitting, *Coord. Chem. Rev.*, 2020, **407**, 213156–213174.
44 B. Singh and A. Indra, Prussian blue- and Prussian blue analogue-derived materials: progress and prospects for electrochemical energy conversion, *Mater. Today Energy*, 2020, **16**, 100404–100428.
45 M. B. Zakaria and T. Chikyow, Recent advances in Prussian blue and Prussian blue analogues: synthesis and thermal treatments, *Coord. Chem. Rev.*, 2017, **352**, 328–345.
46 H. Kim, M. Kim, W. Kim, W. Lee and S. Kim, Photocatalytic enhancement of cesium removal by Prussian blue-deposited TiO_2, *J. Hazard. Mater.*, 2018, **357**, 449–456.
47 Y. Luo, J. Li, X. Liu, L. Tan, Z. Cui, X. Feng, X. Yang, Y. Liang, Z. Li, S. Zhu, Y. Zheng, K. W. K. Yeung, C. Yang, X. Wang and S. Wu, Dual Metal-organic framework heterointerface, *ACS Cent. Sci.*, 2019, **5**, 1591–1601.
48 E. P. Ferreira-Neto, S. Ullah, A. P. Perissinotto, F. S. de Vicente, S. J. L. Ribeiro, M. A. Worsley and U. P. Rodrigues-Filho, Prussian blue as a co-catalyst for enhanced Cr(vi) photocatalytic reduction promoted by titania-based nanoparticles and aerogels, *New J. Chem.*, 2021, **45**, 10217–10231.
49 L. Yuan, C. Zhang, Y. Zou, T. Bao, J. Wang, C. Tang, A. Du, C. Yu and C. Liu, A S–scheme MOF–on–MOF heterostructure, *Adv. Funct. Mater.*, 2023, **33**, 2214627–2214637.
50 C.-H. Su, W.-P. Li, L.-C. Tsao, L.-C. Wang, Y.-P. Hsu, W.-J. Wang, M.-C. Liao, C.-L. Lee and C.-S. Yeh, Enhancing microcirculation on multitriggering manner facilitates angiogenesis and collagen deposition on wound healing by photoreleased NO from Hemin-derivatized colloids, *ACS Nano*, 2019, **13**, 4290–4301.
51 Y.-R. Ji, Y.-F. Guo, X. Liu, P.-F. Wang and T.-F. Yi, Insights on rational design and regulation strategies of Prussian blue analogues and their derivatives towards high-performance electrocatalysts, *Chem. Eng. J.*, 2023, **471**, 144743.
52 X. Li, J. Yu and M. Jaroniec, Hierarchical photocatalysts, *Chem. Soc. Rev.*, 2016, **45**, 2603–2636.

53 Y. Wang, Y. Zhao and Z. Li, 2D covalent organic frameworks as photocatalysts for solar energy utilization, *Macromol. Rapid Commun.*, 2022, **43**, 2200108–2200120.
54 M. Xuan and J. Li, Photosystem II-based biomimetic assembly for enhanced photosynthesis, *Natl. Sci. Rev.*, 2021, **8**, nwab051.
55 H. J. M. Hou, Hydrogen energy production using manganese/semiconductor system inspired by photosynthesis, *Int. J. Hydrogen Energy*, 2017, **1**, 1–9.
56 S. Ye, C. Ding, R. Chen, F. Fan, P. Fu, H. Yin, X. Wang, Z. Wang, P. Du and C. Li, Mimicking the key functions of photosystem II in artificial photosynthesis for photoelectrocatalytic water splitting, *J. Am. Chem. Soc.*, 2018, **140**, 3250–3256.
57 Z. Li, W. Wang, C. Ding, Z. Wang, S. Liao and C. Li, Biomimetic electron transport via multiredox shuttles from photosystem II to a photoelectrochemical cell for solar water splitting, *Energy Environ. Sci.*, 2017, **10**, 765–771.
58 J. H. Kim, H. Kaneko, T. Minegishi, J. Kubota, K. Domen and J. S. Lee, Overall photoelectrochemical water splitting using tandem cell under simulated sunlight, *ChemSusChem*, 2015, **9**, 61–66.
59 K. Wu, K. Li, S. Chen, Y. J. Hou, Y. L. Lu, J. S. Wang, M. J. Wei, M. Pan and C. Y. Su, The redox coupling effect in a photocatalytic RuII–PdII cage with TTF guest as electron relay mediator for visible–light hydrogen–evolving promotion, *Angew. Chem., Int. Ed.*, 2019, **59**, 2639–2643.
60 P. Lin, J. Shen, H. Tang, Zulfiqar, Z. Lin and Y. Jiang, Enhanced photocatalytic H_2 evolution of ultrathin g-C_3N_4 nanosheets via surface shuttle redox, *J. Alloys Compd.*, 2019, **810**, 151918–151928.
61 R. Abe, M. Higashi and K. Domen, Overall water splitting under visible light through a two–step photoexcitation between TaON and WO_3 in the presence of an iodate-iodide shuttle redox mediator, *ChemSusChem*, 2011, **4**, 228–237.
62 Y. Wang, H. Suzuki, J. Xie, O. Tomita, D. J. Martin, M. Higashi, D. Kong, R. Abe and J. Tang, Mimicking natural photosynthesis: Solar to renewable H_2 fuel synthesis by Z-scheme water splitting systems, *Chem. Rev.*, 2018, **118**, 5201–5241.
63 S. Liang, M. Jiang, H. Luo, Y. Ma and J. Yang, A high–rate electrode with grotthuss topochemistry for membrane–free decoupled acid water electrolysis, *Adv. Energy Mater.*, 2021, **11**, 2102057–2102067.
64 L. Guo, H. Huang, L. Mei, M. Li and Y. Zhang, Bismuth-based Z-scheme photocatalytic systems for solar energy conversion, *Mater. Chem. Front.*, 2021, **5**, 2484–2505.
65 B. You and Y. Sun, Innovative strategies for electrocatalytic water splitting, *Acc. Chem. Res.*, 2018, **51**, 1571–1581.
66 M. Yasuda, T. Matsumoto and T. Yamashita, Sacrificial hydrogen production over TiO_2-based photocatalysts: Polyols, carboxylic acids, and saccharides, *Renewable Sustainable Energy Rev.*, 2018, **81**, 1627–1635.
67 K. Sun, J. Shen, Q. Liu, H. Tang, M. Zhang, S. Zulfiqar and C. Lei, Synergistic effect of Co(II)-hole and Pt-electron cocatalysts for enhanced photocatalytic hydrogen evolution performance of P-doped g-C_3N_4, *Chin. J. Catal.*, 2020, **41**, 72–81.
68 F. A. Rahimi, S. Dey, P. Verma and T. K. Maji, Photocatalytic CO_2 reduction based on a Re(I)-integrated conjugated microporous polymer: role of a sacrificial electron donor in product selectivity and efficiency, *ACS Catal.*, 2023, **13**, 5969–5978.
69 F. M. Zhang, J. L. Sheng, Z. D. Yang, X. J. Sun, H. L. Tang, M. Lu, H. Dong, F. C. Shen, J. Liu and Y. Q. Lan, Rational design of MOF/COF hybrid materials for photocatalytic H_2 evolution in the presence of sacrificial electron donors, *Angew. Chem., Int. Ed.*, 2018, **57**, 12106–12110.
70 C. Mo, M. Yang, F. Sun, J. Jian, L. Zhong, Z. Fang, J. Feng and D. Yu, Alkene–linked covalent organic frameworks boosting photocatalytic hydrogen evolution by efficient charge separation and transfer in the presence of sacrificial electron donors, *Adv. Sci.*, 2020, **7**, 1902988–1902996.
71 H. Bahruji, M. Bowker, P. R. Davies and F. Pedrono, New insights into the mechanism of photocatalytic reforming on Pd/TiO_2, *Appl. Catal., B*, 2011, **107**, 205–209.
72 J.-D. Xiao, Q. Shang, Y. Xiong, Q. Zhang, Y. Luo, S.-H. Yu and H.-L. Jiang, Boosting photocatalytic hydrogen production of a metal-organic framework decorated with platinum nanoparticles: The platinum location matters, *Angew. Chem., Int. Ed.*, 2016, **55**, 1–6.
73 J. Wang, C. Qiu, S. Zhao, M. Guan, H. Yu, Z. Chen, B. Lu, B. Wanyan, L. Zhang and J. Shu, Ultra-stable Cu-ion-exchanged cobalt hexacyanoferrate(ii) in aqueous copper-ion storage, *Inorg. Chem. Front.*, 2024, **11**, 1108–1116.
74 A. Sartorel, M. Bonchio, S. Campagna and F. Scandola, Tetrametallic molecular catalysts for photochemical water oxidation, *Chem. Soc. Rev.*, 2013, **42**, 2262–2280.
75 J. Twilton, C. Le, P. Zhang, M. H. Shaw, R. W. Evans and D. W. C. MacMillan, The merger of transition metal and photocatalysis, *Nat. Rev. Chem.*, 2017, **1**, 1–19.
76 J. Follana-Berná, R. Farran, W. Leibl, A. Quaranta, Á. Sastre-Santos and A. Aukauloo, Phthalocyanine as a bioinspired model for chlorophyll f-containing photosystem II drives photosynthesis into the far–red region, *Angew. Chem., Int. Ed.*, 2021, **60**, 12284–12288.
77 X. Han, X. Ge, W.-W. He, W. Shen, T. Zhou, J.-S. Wang, R.-L. Zhong, A. M. Al-Enizi, A. Nafady and S. Ma, Covalent triazine frameworks modified by ultrafine Pt nanoparticles for efficient photocatalytic hydrogen production, *Nano Res.*, 2024, DOI: **10.1007/s12274-024-6483-y**.
78 R. Li, C. Zhang, K. You, B. Li, W. Bu, X. Meng, B. Ma and Y. Ding, Molecular confined synthesis of magnetic CoO_x/Co/C hybrid catalyst for photocatalytic water oxidation and CO_2 reduction, *Chin. Chem. Lett.*, 2023, **34**, 108801–108806.
79 Q. Han, D. Sun, J. Zhao, X. Liang and Y. Ding, A novel dicobalt-substituted tungstoantimonate polyoxometalate: Synthesis, characterization, and photocatalytic water oxidation properties, *Chin. J. Catal.*, 2019, **40**, 953–958.

80 W. Sun, J. Zhu, M. Zhang, X. Meng, M. Chen, Y. Feng, X. Chen and Y. Ding, Recent advances and perspectives in cobalt-based heterogeneous catalysts for photocatalytic water splitting, CO_2 reduction, and N_2 fixation, *Chin. J. Catal.*, 2022, **43**, 2273–2300.

81 W. Li, A. Elzatahry, D. Aldhayan and D. Zhao, Core-shell structured titanium dioxide nanomaterials for solar energy utilization, *Chem. Soc. Rev.*, 2018, **47**, 8203–8237.

82 M. Kaneko and A. Yamada, Photoresponsive graphite electrode coated with bilayer membranes of prussian blue and polymer-pendant $Ru(bpy)_3^{2+}$, *Electrochim. Acta*, 1986, **31**, 273–275.

83 T. Shirakawa, M. Higashi, O. Tomita and R. Abe, Surface-modified metal sulfides as stable H_2-evolving photocatalysts in Z-scheme water splitting with a $[Fe(CN)_6]^{3-/4-}$ redox mediator under visible-light irradiation, *Sustainable Energy Fuels*, 2017, **1**, 1065–1073.

84 H. Kitano, A. Kobayashi, M. Yoshida and M. Kato, Photocatalytic hydrogen evolution driven by platinated CdS nanorods with a hexacyanidoruthenate redox mediator, *Sustainable Energy Fuels*, 2018, **2**, 2609–2615.

85 H. Matsuoka, T. Inoue, H. Suzuki, O. Tomita, S. Nozawa, A. Nakada and R. Abe, Surface modification with metal hexacyanoferrates for expanding the choice of H_2-evolving photocatalysts for both Fe^{3+}/Fe^{2+} redox–mediated and interparticle Z–scheme water–splitting systems, *Sol. RRL*, 2023, **7**, 2300431.

86 T. Inoue, T. Watanabe, A. Fujishima and K. Honda, Suppression of surface dissolution of CdS photoanode by reducing agents, *J. Electrochem. Soc.*, 1977, **124**, 719–722.

87 J. R. Darwent, H_2 production photosensitized by aqueous semiconductor dispersions, *J. Chem. Soc., Faraday Trans. 2*, 1981, **77**, 1703–1709.

88 M. Matsumura, Y. Saho and H. Tsubomura, Photocatalytic hydrogen production from solutions of sulfite using platinized cadmium sulfide powder, *J. Phys. Chem.*, 1983, **87**, 3807–3808.

89 Q. Zhu, Q. Xu, M. Du, X. Zeng, G. Zhong, B. Qiu and J. Zhang, Recent progress of metal sulfide photocatalysts for solar energy conversion, *Adv. Mater.*, 2022, **34**, 2202929–2202945.

90 Y. Su, D. Ao, H. Liu and Y. Wang, MOF-derived yolk-shell CdS microcubes with enhanced visible-light photocatalytic activity and stability for hydrogen evolution, *J. Mater. Chem. A*, 2017, **5**, 8680–8689.

91 P. Zhang, D. Luan and X. W. Lou, Fabrication of CdS frame–in–cage particles for efficient photocatalytic hydrogen generation under visible–light irradiation, *Adv. Mater.*, 2020, **32**, 2004561–2004567.

92 J. Nai and X. W. Lou, Hollow structures based on Prussian blue and its analogs for electrochemical energy storage and conversion, *Adv. Mater.*, 2018, **31**, 1706825–1706844.

93 J. Lu, L. Cheng, J. Li and H. Liu, MOF-derived strategy for monodisperse $Cd_{0.5}Zn_{0.5}S$ nanospheres with enhanced photocatalytic activity for hydrogen evolution, *J. Alloys Compd.*, 2020, **849**, 156669–156679.

94 Y. Li, Y. Li, Z. Jin and N. Tsubaki, Etching $C_6CoK_3N_6$-induced ZnCdS for improved hydrogen evolution, *Sustainable Energy Fuels*, 2022, **6**, 408–419.

95 Y. Li, Z. Jin and N. Tsubaki, Distinctive synthesis of CdS-based photocatalysts based on a Prussian blue analog induction strategy for efficient solar-driven water splitting applications, *J. Mater. Chem. C*, 2022, **10**, 18213–18225.

96 X. Cao, L. Zhang, C. Guo, T. Chen, C. Feng, Z. Liu, Y. Qi, W. Wang and J. Wang, Ni-doped CdS porous cubes prepared from prussian blue nanoarchitectonics with enhanced photocatalytic hydrogen evolution performance, *Int. J. Hydrogen Energy*, 2022, **47**, 3752–3761.

97 Y. Yang, C. Zhou, W. Wang, W. Xiong, G. Zeng, D. Huang, C. Zhang, B. Song, W. Xue, X. Li, Z. Wang, D. He, H. Luo and Z. Ouyang, Recent advances in application of transition metal phosphides for photocatalytic hydrogen production, *Chem. Eng. J.*, 2021, **405**, 126547.

98 Z. Hu, X. Hao and Z. Jin, Morphology engineering ultrathin nitrogen-doped carbon Co-FeP derived from Co-Fe Prussian blue Analogs for wide spectrum photocatalytic H_2 evolution, *Fuel*, 2023, **333**, 126336.

99 Y. Li, Z. Jin and N. Tsubaki, Chemical etching and phase transformation of Nickel-Cobalt Prussian blue analogs for improved solar-driven water-splitting applications, *J. Colloid Interface Sci.*, 2023, **641**, 861–874.

100 R. Lv, Z. Guo, X. Hou, X. Wu, K. Huang and S. Feng, Exsolution: A promising strategy for constructing advanced composite solids, *Mater. Today Sustainability*, 2022, **19**, 100172.

101 P. Acevedo Peña, D. Ramírez Ortega, D. Guerrero Araque, A. Hernández Gordillo, R. Zanella and E. Reguera, Boosting the photocatalytic hydrogen production of TiO_2 by using copper hexacyanocobaltate as co-catalyst, *Int. J. Hydrogen Energy*, 2021, **46**, 10312–10323.

102 C. Shi, S. Ye, X. Wang, F. Meng, J. Liu, T. Yang, W. Zhang, J. Wei, N. Ta, G. Q. Lu, M. Hu and J. Liu, Modular construction of Prussian blue analog and TiO_2 dual–compartment Janus nanoreactor for efficient photocatalytic water splitting, *Adv. Sci.*, 2021, **8**, 2001987.

103 W. Qi, S. Liu, F. Li, H. Jiang, Z. Cheng, S. Zhao and M. Yang, Prussian blue derived Fe_2N for efficiently improving the photocatalytic hydrogen evolution activity of g-C_3N_4 nanosheets, *Catal. Sci. Technol.*, 2019, **9**, 2571–2577.

104 H. Xie, K. Wang, D. Xiang, S. Li and Z. Jin, Enwrapping graphdiyne (g-C_nH_{2n-2}) on hollow $NiCo_2O_4$ nanocages derived from a Prussian blue analogue as a p-n heterojunction for highly efficient photocatalytic hydrogen evolution, *J. Mater. Chem. A*, 2023, **11**, 14971–14989.

105 W. Wang, J. Chen, C. Li and W. Tian, Achieving solar overall water splitting with hybrid photosystems of photosystem II and artificial photocatalysts, *Nat. Commun.*, 2014, **5**, 5647–5655.

106 M. Zhang, Y. Chen, J.-N. Chang, C. Jiang, W.-X. Ji, L.-Y. Li, M. Lu, L.-Z. Dong, S.-L. Li, Y.-P. Cai and Y.-Q. Lan, Efficient charge migration in chemically-bonded Prussian

blue analogue/CdS with beaded structure for photocatalytic H_2 evolution, *JACS Au*, 2021, **1**, 212–220.

107 X. Guo, L. Fan, T. Yang, Y. Liu and Z. Jin, CdS nanorods and ZnCd-PBA construct a direct S-scheme heterojunction for efficient photocatalytic hydrogen evolution, *J. Phys. Chem. C*, 2023, **127**, 15096–15106.

108 K. Wang, H. Xie, Y. Li, G. Wang and Z. Jin, Anchoring highly-dispersed ZnCdS nanoparticles on NiCo Prussian blue analogue-derived cubic-like NiCoP forms an S-scheme heterojunction for improved hydrogen evolution, *J. Colloid Interface Sci.*, 2022, **628**, 64–78.

109 Y. Li, Z. Jin and N. Tsubaki, Hollow ZnCdS and NiCoP nanostructures for photocatalytic hydrogen generation, *ACS Appl. Nano Mater.*, 2022, **5**, 14677–14688.

110 C. Q. Li, X. Du, S. Jiang, Y. Liu, Z. L. Niu, Z. Y. Liu, S. S. Yi and X. Z. Yue, Constructing direct Z–scheme heterostructure by enwrapping $ZnIn_2S_4$ on CdS hollow cube for efficient photocatalytic H_2 generation, *Adv. Sci.*, 2022, **9**, 2201773.

111 X. Meng, S. Wang, C. Zhang, C. Dong, R. Li, B. Li, Q. Wang and Y. Ding, Boosting hydrogen evolution performance of a CdS-based photocatalyst: In situ transition from type I to type II heterojunction during photocatalysis, *ACS Catal.*, 2022, **12**, 10115–10126.

112 T. G. Ulusoy Ghobadi, E. Ozbay and F. Karadas, How to build Prussian blue based water oxidation catalytic assemblies: Common trends and strategies, *Chem. – Eur. J.*, 2021, **27**, 3638–3649.

113 P. A. Christensen, A. Harriman, P. Neta and M.-C. Richoux, Photo-oxidation of water using Prussian blue as catalyst, *J. Chem. Soc., Faraday Trans. 1*, 1985, **81**, 2461–2466.

114 S. Goberna-Ferrón, W. Y. Hernández, B. Rodríguez-García and J. R. Galán-Mascarós, Light-driven water oxidation with metal hexacyanometallate heterogeneous catalysts, *ACS Catal.*, 2014, **4**, 1637–1641.

115 Y. Yamada, K. Oyama, R. Gates and S. Fukuzumi, High catalytic activity of heteropolynuclear cyanide complexes containing cobalt and platinum ions: Visible–light driven water oxidation, *Angew. Chem., Int. Ed.*, 2015, **54**, 5613–5617.

116 Y. Yamada, K. Oyama, T. Suenobu and S. Fukuzumi, Photocatalytic water oxidation by persulphate with a Ca^{2+} ion-incorporated polymeric cobalt cyanide complex affording O_2 with 200% quantum efficiency, *Chem. Commun.*, 2017, **53**, 3418–3421.

117 T. G. Ulusoy Ghobadi, E. Akhuseyin Yildiz, M. Buyuktemiz, S. Sadigh Akbari, D. Topkaya, Ü. İsci, Y. Dede, H. G. Yaglioglu and F. Karadas, A noble–metal–free heterogeneous photosensitizer–relay catalyst triad that catalyzes water oxidation under visible light, *Angew. Chem., Int. Ed.*, 2018, **57**, 17173–17177.

118 Z. Kap and F. Karadas, Visible light-driven water oxidation with a ruthenium sensitizer and a cobalt-based catalyst connected with a polymeric platform, *Faraday Discuss.*, 2019, **215**, 111–122.

119 A. A. Ahmad, T. G. Ulusoy Ghobadi, M. Buyuktemiz, E. Ozbay, Y. Dede and F. Karadas, Light-driven water oxidation with ligand-engineered Prussian blue analogues, *Inorg. Chem.*, 2022, **61**, 3931–3941.

120 R. Chalil Oglou, T. G. Ulusoy Ghobadi, E. Ozbay and F. Karadas, "Plug and Play" photosensitizer-catalyst dyads for water oxidation, *ACS Appl. Mater. Interfaces*, 2022, **14**, 21131–21140.

121 Y. Feng, J. Wei and Y. Ding, Efficient photochemical, thermal, and electrochemical water oxidation catalyzed by a porous iron-based oxide derived metal-organic framework, *J. Phys. Chem. C*, 2015, **120**, 517–526.

122 Y. Dong, T. Tian, C. Xu, K. Ma, W. Sun and Y. Ding, Cubic Co-Co prussian blue MOF-based transition metal phosphide as an efficient catalyst for visible light-driven water oxidation, *J. Catal.*, 2020, **382**, 13–21.

123 J. Guo, H. Li, D. Wang, L. Zhang, Y. Ma, N. Akram, Y. Zhang and J. Wang, Efficient difunctional photocatalyst prepared in situ from Prussian blue analogues for catalytic water oxidation and visible-light absorption, *Catal. Sci. Technol.*, 2018, **8**, 6375–6383.

124 G. Gundogdu, T. G. Ulusoy Ghobadi, S. Sadigh Akbari, E. Ozbay and F. Karadas, Photocatalytic water oxidation with a Prussian blue modified brown TiO_2, *Chem. Commun.*, 2021, **57**, 508–511.

125 S. S. Akbari and F. Karadas, Precious metal–free photocatalytic water oxidation by a layered double hydroxide–Prussian blue analogue hybrid assembly, *ChemSusChem*, 2020, **14**, 679–685.

126 S. S. Akbari, U. Unal and F. Karadas, Photocatalytic water oxidation with a CoFe Prussian blue analogue-layered niobate hybrid material, *ACS Appl. Energy Mater.*, 2021, **4**, 12383–12390.

127 X. Meng, S. Xu, C. Zhang, P. Feng, R. Li, H. Guan and Y. Ding, Prussian blue type cocatalysts for enhancing the photocatalytic water oxidation performance of $BiVO_4$, *Chem. – Eur. J.*, 2022, **28**, e202201407.

128 X. Yang, K. Li, G. Wang, X. Li, P. Zhou, S. Ding, Z. Lyu, Y. C. Chang, Y. Zhou and W. Zhu, 2D Catalysts for CO_2 photoreduction: Discussing structure efficiency strategies and prospects for scaled production based on current progress, *Chem. – Eur. J.*, 2022, **28**, e202201881.

129 S. Wang, X. Han, Y. Zhang, N. Tian, T. Ma and H. Huang, Inside–and–out semiconductor engineering for CO_2 photoreduction: From recent advances to new trends, *Small Struct.*, 2020, **2**, 2000061.

130 L. Zhang and J. Zhang, Metal-organic frameworks for CO_2 photoreduction, *Front. Energy*, 2019, **13**, 221–250.

131 J. Zhou, J. Li, L. Kan, L. Zhang, Q. Huang, Y. Yan, Y. Chen, J. Liu, S.-L. Li and Y.-Q. Lan, *Nat. Commun.*, 2022, **13**, 4681–4691.

132 F. Karadas, H. El-Faki, E. Deniz, C. T. Yavuz, S. Aparicio and M. Atilhan, CO_2 adsorption studies on Prussian blue analogues, *Microporous Mesoporous Mater.*, 2012, **162**, 91–97.

133 J. Nai, S. Wang and X.-W. (David) Lou, Ordered colloidal clusters constructed by nanocrystals with valence for efficient CO_2 photoreduction, *Sci. Adv.*, 2019, **5**, eaax5095.

134 X. Meng, J. Yang, C. Zhang, Y. Fu, K. Li, M. Sun, X. Wang, C. Dong, B. Ma and Y. Ding, Light-driven CO_2 reduction over Prussian blue analogues as heterogeneous catalysts, *ACS Catal.*, 2021, **12**, 89–100.

135 S. Zhu, N. Li, D. Zhang and T. Yan, Metal/oxide heterostructures derived from Prussian blue analogues for efficient photocatalytic CO_2 hydrogenation to hydrocarbons, *J. CO_2 Util.*, 2022, **64**, 102117–102128.

136 S. Zhao, C. Li, K. Ren, Z. Fang, P. Fang, Y. Zhu and P. Fang, Ternary Ni-Co-Fe oxides based on Prussian blue analog for efficient photothermal catalytic CO_2 reduction to CO and CH_4, *Appl. Catal., A*, 2023, **655**, 119109–119120.

137 M. Lin, W. Jiang, T. Zhang, B. Yang, Z. Zhuang and Y. Yu, Ordered CoIII–MOF@CoII–MOF heterojunction for highly efficient photocatalytic syngas production, *Small Sci.*, 2023, **3**, 2200085.

138 M. Lin, R. Cao, Y. Luo, T. Zhang, Z. Zhuang and Y. Yu, Built-in electric field directs electron transport at ultrathin $Ni(OH)_2$/metal-organic framework interface for efficient photocatalytic CO_2 reduction, *ACS Appl. Energy Mater.*, 2022, **5**, 2161–2168.

139 W. Wu, Y. Wu, Z. Zhang, L. Sun, R. Wei, J. Zhang, L. Gao, X. Pan, J. Yu and G. Xiao, Multichannel electron transmission and multiple light scattering in CoCo PBA/$CoSn(OH)_6$/Pt photocatalyst for effective conversion of simulated flue gas, *Fuel*, 2023, **334**, 126747–126756.

140 B. Li, M. Chen, Q. Hu, J. Zhu, X. Yang, Z. Li, C. Hu, Y. Li, P. Ni and Y. Ding, Facilely tunable dodecahedral polyoxometalate framework loaded with mono- or bimetallic sites for efficient photocatalytic CO_2 reduction, *Appl. Catal., B*, 2024, **346**, 123733–123746.

